JGR Atmospheres

RESEARCH ARTICLE
10.1029/2019JD031740

Seasonal Variations in Western North Atlantic Remote Marine Aerosol Properties

P.K. Quinn[1], T.S. Bates[2,1], D.J. Coffman[1], L. Upchurch[2,1], J.E. Johnson[2,1], R. Moore[3], L. Ziemba[3], T.G. Bell[4], E.S. Saltzman[5], J. Graff[6], and M.J. Behrenfeld[6]

[1]PMEL, NOAA, Seattle, WA, USA, [2]JISAO, University of Washington, Seattle, WA, USA, [3]NASA Langley, Hampton, VA, USA, [4]Plymouth Marine Sciences Laboratory, Plymouth, UK, [5]Department of Chemistry, University of California, Irvine, CA, USA, [6]Department of Botany and Plant Pathology, Oregon State University, Corvallis, OR, USA

Key Points:
- Nonvolatile material in the Aitken mode after heating to 230 °C occurs in all seasons likely due to downward mixing from aloft
- Nonsea salt sulfate links the phytoplankton bloom to cloud condensation nuclei (CCN) during bloom climax
- Sea spray aerosol only makes up a significant fraction of CCN in November when phytoplankton bloom accumulation has not begun

Correspondence to:
P. K. Quinn,
patricia.k.quinn@noaa.gov

Citation:
Quinn, P. K., Bates, T. S., Coffman, D. J., Upchurch, L., Johnson, J. E., Moore, R., et al. (2019). Seasonal variations in western North Atlantic remote marine aerosol properties. *Journal of Geophysical Research: Atmospheres*, *124*, 14,240–14,261. https://doi.org/10.1029/2019JD031740

Received 26 SEP 2019
Accepted 11 DEC 2019
Accepted article online 13 DEC 2019
Published online 27 DEC 2019

Author Contributions:
Conceptualization: P.K. Quinn, T.S. Bates, R. Moore
Data curation: D.J. Coffman, L. Upchurch, J.E. Johnson, R. Moore, L. Ziemba, T.G. Bell, E.S. Saltzman, J. Graff, M.J. Behrenfeld
Formal analysis: P.K. Quinn
Investigation: P.K. Quinn, T.S. Bates, D.J. Coffman, L. Upchurch, L. Ziemba, J. Graff, M.J. Behrenfeld
Methodology: P.K. Quinn, T.S. Bates, D.J. Coffman, L. Upchurch, J.E. Johnson, L. Ziemba, T.G. Bell, E.S. Saltzman, M.J. Behrenfeld
Software: D.J. Coffman
Writing - original draft: P.K. Quinn
Writing – review & editing: T.S. Bates, R. Moore, E.S. Saltzman, J. Graff, M.J. Behrenfeld

Abstract The impact of ocean ecosystems on marine boundary layer aerosols and clouds has been the subject of much research but remains uncertain. Five experiments were recently conducted in the western North Atlantic to assess if the seasonally recurring phytoplankton bloom affects aerosol properties. These experiments include the second Western Atlantic Climate Study and four North Atlantic Aerosols and Marine Ecosystem Study cruises. Measurements of unheated and heated number size distributions, cloud condensation nucleus (CCN) concentrations, and aerosol composition were used to identify primary and secondary aerosol components that could be related to the state of the bloom. Only periods of clean marine air, as defined by radon, particle number concentrations, aerosol light absorption coefficient, and back trajectories, were included in the analysis. Nonvolatile material was found to be prevalent in the Aitken mode size range after heating to 230°, likely due to downward mixing from the free troposphere. CCN concentrations at 0.1% supersaturation were best correlated ($r^2 = 0.73$) with accumulation mode nss $SO_4^=$. Sea spray aerosol was only correlated with CCN during November when bloom accumulation had not yet occurred and dimethylsulfide concentrations were at a minimum. The fraction of CCN attributable to sea spray aerosol was less than 20% during March, May/June, and September, indicating the limited contribution of sea spray aerosol to the CCN population of the western North Atlantic atmosphere. The strongest link between the plankton bloom and aerosol and cloud properties appears to be due to biogenic non-sea salt $SO_4^=$.

1. Introduction

Ocean phytoplankton productivity is an integral part of many Earth system processes. It drives the exchange of CO_2 between the ocean and atmosphere and forms the basis for ocean food webs (Siegal et al., 2014; Takahashi et al., 2009). In addition to the impacts of plankton productivity on ocean ecosystems, it has been hypothesized to lead to the emission of high levels of aerosol-forming compounds (Gondwe et al., 2003; O'Dowd et al., 2004) that can affect cloud formation and alter Earth's radiation budget (Andreae & Rosenfeld, 2008). The surface ocean is projected to warm by 1.3 to 2.8 °C globally over the twenty-first century (Bopp et al., 2013). Impacts of this warming on plankton blooms, ocean ecosystems, and ocean-to-atmosphere fluxes of aerosols and their precursor gases are highly uncertain. A fundamental understanding of linkages between surface ocean ecosystems and ocean-derived aerosols is required to address this uncertainty. One approach for improved understandings of these linkages is simultaneous measurements of relevant surface ocean and aerosol properties in an ocean region with seasonally varying plankton blooms and a minimally polluted overlying atmosphere.

The western North Atlantic is such a region. It hosts the largest annual phytoplankton bloom in the global ocean with a large spatial and seasonal variability in plankton biomass and composition (Behrenfeld et al., 2019). In addition, periods of low aerosol number concentrations associated with unpolluted air masses allow for the detection of any potential impacts of the bloom on aerosol properties (Pennypacker & Wood, 2017). Five experiments were conducted in the western North Atlantic between 2014 and 2018 with the objective of finding links between the bloom and marine aerosols. These experiments include the second Western Atlantic Climate Study (WACS-2) and four North Atlantic Aerosol and Marine Ecosystem Study (NAAMES) cruises. Cruise tracks and dates for the WACS-2 and NAAMES experiments are shown in Figure 1. This series of cruises was the first time the western North Atlantic bloom was systematically

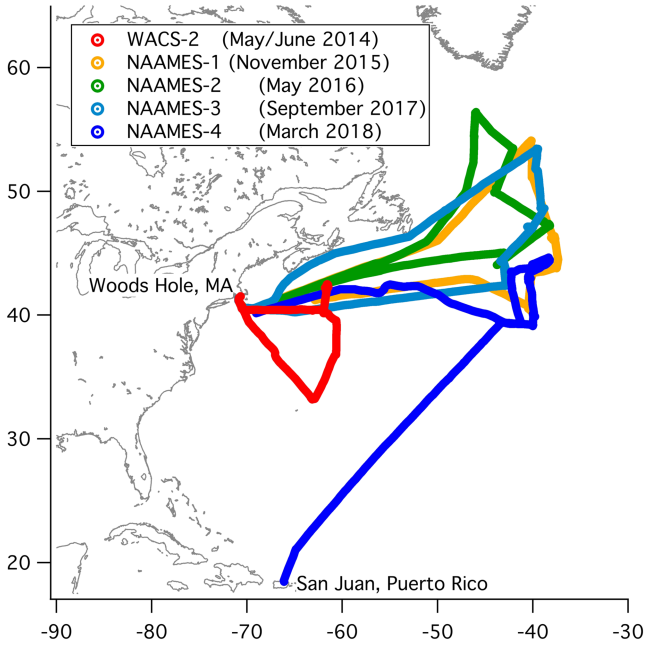

Figure 1. Cruise tracks and timing for WACS-2 and NAAMES-1, NAAMES-2, NAAMES-3, and NAAMES-4.

sampled during every season with extensive ocean and atmosphere measurements able to assess how changes in the state of the bloom might impact ocean-derived aerosol properties. Potential direct links between bloom state and aerosol properties include increased concentrations of phytoplankton-derived dimethylsulfide (DMS) leading to higher concentrations of nss $SO_4^=$ aerosol (Pandis et al., 1994) and changes in composition or concentration of seawater organic matter that could impact marine aerosol composition and CCN activity (Hawkins & Russell, 2010; Rinaldi et al., 2010).

The North Atlantic plankton bloom begins in late autumn. At this time, phytoplankton division rates are decreasing because of decreasing incident sunlight and a deepening mixed layer. However, the deepening mixed layer also impacts the community of predators feeding on the phytoplankton because the mixing dilutes both predator and prey populations over an increasing volume of water. Bloom initiation happens when the dilution effect on predator-prey encounter rates is more severe than the impact of lower mixed layer light levels on phytoplankton division rates (Behrenfeld, 2010; Behrenfeld et al., 2013; Boss & Behrenfeld, 2010). Once the mixed layer stops deepening in early spring, the concentration of phytoplankton per unit volume of seawater starts to increase (i.e., the population is no longer being diluted). When this happens, the predator population responds and would rapidly catch up to the phytoplankton and terminate the bloom if phytoplankton division rates remained constant. However, during this spring period the mixed layer continues to become more shallow and incident light continues to increase, which allows phytoplankton division rates to accelerate. It is this acceleration in division rate that perpetuates the bloom because it allows the phytoplankton to remain ahead of the rapidly rising loss rates, which exhibit a time-lagged response to increasing prey abundance (Behrenfeld & Boss, 2018). The ultimate outcome of this seasonal process is a bloom climax in late spring or early summer that is terminated by either a depletion of mixed layer nutrients or the achievement of maximum phytoplankton division rates. This ecosystem-based view of the seasonality of the plankton bloom suggests that harsher winter conditions (colder temperatures and deeper mixing) lead to greater plankton biomass while milder winters will lead to less biomass (Behrenfeld et al., 2019), potentially having the consequential effect of impacting overlying marine aerosol properties.

One overarching goal of NAAMES was to define linkages between ocean ecosystem properties and atmospheric aerosols to improve predictions of marine aerosol-cloud-climate interactions for a warmer future ocean. A starting point in addressing this goal is determining if there are detectable changes in ocean-derived aerosols in response to seasonal changes in the bloom state. In this work, we report observations of ambient aerosol properties measured across all seasons in the western Atlantic under clean marine conditions as defined by low radon (a tracer of continental air masses; <500 mBq m^{-3}), low total particle number concentration (<1,000 cm^{-3}), low aerosol light absorption coefficient (<0.2 Mm^{-1}), and HYSPLIT back trajectories that indicated no transport from anthropogenic source regions for at least four days prior to reaching the ship's location (Stein et al., 2015). The aerosol properties used in the analysis include unheated and heated (230 °C) number and volume size distributions, CCN activity, and aerosol composition. Results from WACS-2 and all four NAAMES cruises are presented.

2. Methods

2.1. Aerosol Sampling Inlet

Sample air for all aerosol measurements was drawn through a 5-m mast. The entrance to the mast was 18 m above sea level and forward of the ship's stack. The mast inlet was automatically rotated into the relative wind to maintain nominally isokinetic flow. Air entered the inlet through a 5-cm-diameter hole, passed through a 7° expansion cone, and then into the 20-cm inner diameter sampling mast. The flow through

the mast was 1 m^3 min^{-1}. The transmission efficiency of the inlet for particles with aerodynamic diameters less than 6.5 μm is greater than 95% (Bates et al., 2002).

When the ambient relative humidity (RH) was high (~80%), due to warm sea surface and atmospheric temperatures, the bottom 1.5 m of the mast was heated to establish a stable reference RH for the sample air of 60 ± 5%. On average, the aerosol was heated above ambient temperature by 9.1 ± 1.8 °C, 10 ± 2.6 °C, 16 ± 2.6 °C, 16 ± 2.5 °C, and 7.7 ± 2.7 °C for NAAMES-1, NAAMES-2, NAAMES-3, NAAMES-4, and WACS-2, respectively. During periods of low ambient RH (between 20 and 40%), due to cold sea surface and atmospheric temperatures, no heating was applied to the sample air. Stainless steel tubes extending into the heated portion of the mast were connected to downstream aerosol instrumentation with either conductive silicone tubing or stainless steel tubing for analysis of organic aerosol. The data reported here are based on air that was sampled only when the particle number concentration, the relative wind speed, and the relative wind direction all indicated that there was no possibility of contamination from the ship's stack.

2.2. Aerosol Number Concentration

One of the mast tubes was used to supply ambient air to two different particle counters. A TSI 3785 condensation nucleus (CN) counter was used to determine the number concentration of particles with geometric mean diameter (D_{gn}) >5 nm (CN_5) in diameter. A TSI 3010 was used to determine the number concentration of particles with D_{gn} >13 nm (CN_{13}). The ratio of CN_5/CN_{13} was used as an indicator of the presence of newly formed particles (Bates et al., 1998; Figure 2).

2.3. Aerosol Volatility at 230 °C

One of the mast tubes was used to supply air to a thermodenuder (Wehner et al., 2002)—Scanning Mobility Particle Sizer (SMPS) system (Bates et al., 2012). A 30-L min^{-1} flow passed through a multijet cascade impactor with a 50% aerodynamic cutoff diameter (D_{aero}) of 1.1 μm (Berner et al., 1979) at the sample RH detailed in section 2.1 and was then subsampled at 5 L min^{-1}. The impactor, as with all impactors described here, also contained a 10-μm jet plate to minimize the bounce of large particles onto lower stages. The subsampled flow was drawn into two 2.2-cm inner diameter tubes, one at ambient temperature and one heated to 230 °C. The heated section was 0.61 m long resulting in a residence time in the heated tube of 2.8 s. At the end of the heated tube, the flow passed through a perforated stainless steel tube (0.55 m) surrounded by a sheet of carbon-impregnated paper to remove the reactive gas phase species. The heated and unheated airflows were then isokinetically subsampled at the centerline at 2.0 L min^{-1} and passed through a nafion dryer. A valve switched the two flows every 5 min so that either the heated or the unheated sample entered the SMPS while the other flow went to a bypass line. Using one SMPS for both the heated and unheated sample prevented uncertainties due to differences in SMPS instruments. Size distributions were measured between 0.02 and 0.5 μm D_{gn}. In addition to the SMPS, the flows were sampled with a CN counter (TSI 3010) and CCN counter (Droplet Measurement Technologies (DMT)) for a measure of heated and unheated total particle number and CCN concentrations, respectively. Heated and unheated volume size distributions were calculated from the measured number size distributions. Tests with ammonium sulfate aerosol showed that less than 10% of the total particle number concentration was reformed between the denuder and the SMPS with all of the reformation occurring at particle diameters less than 0.03 μm. This portion of the unheated and heated number size distributions (D_{gn} <0.03 μm) was omitted from the analysis.

2.4. Aerosol Number Size Distribution

In addition to heated and unheated size distributions measured with the SMPS, number size distributions from 0.02 to 10 μm were measured with a combination of three particle sizers. One of the mast tubes was used to supply air at the sample RH detailed in section 2.1 to a short column differential mobility particle sizer (Aitken-DMPS), a medium column differential mobility particle sizer (Accumulation-DMPS), and an aerodynamic particle sizer (APS, TSI 3321). The Aitken-DMPS was a short column University of Vienna (Winklmeyer et al., 1991) instrument connected to a TSI 3760A particle counter operating with a positive center rod voltage to sample particles with a negative charge. Data were collected in 10 size bins from 0.02 to 0.2 μm D_{gn}. The Aitken-DMPS operated with an aerosol flow rate of 1 L min^{-1} and a sheath air flow rate of 10 L min^{-1}. The Accumulation-DMPS was a medium column University of Vienna instrument connected to a TSI 3760A particle counter operating with a positive center rod voltage to sample particles with a

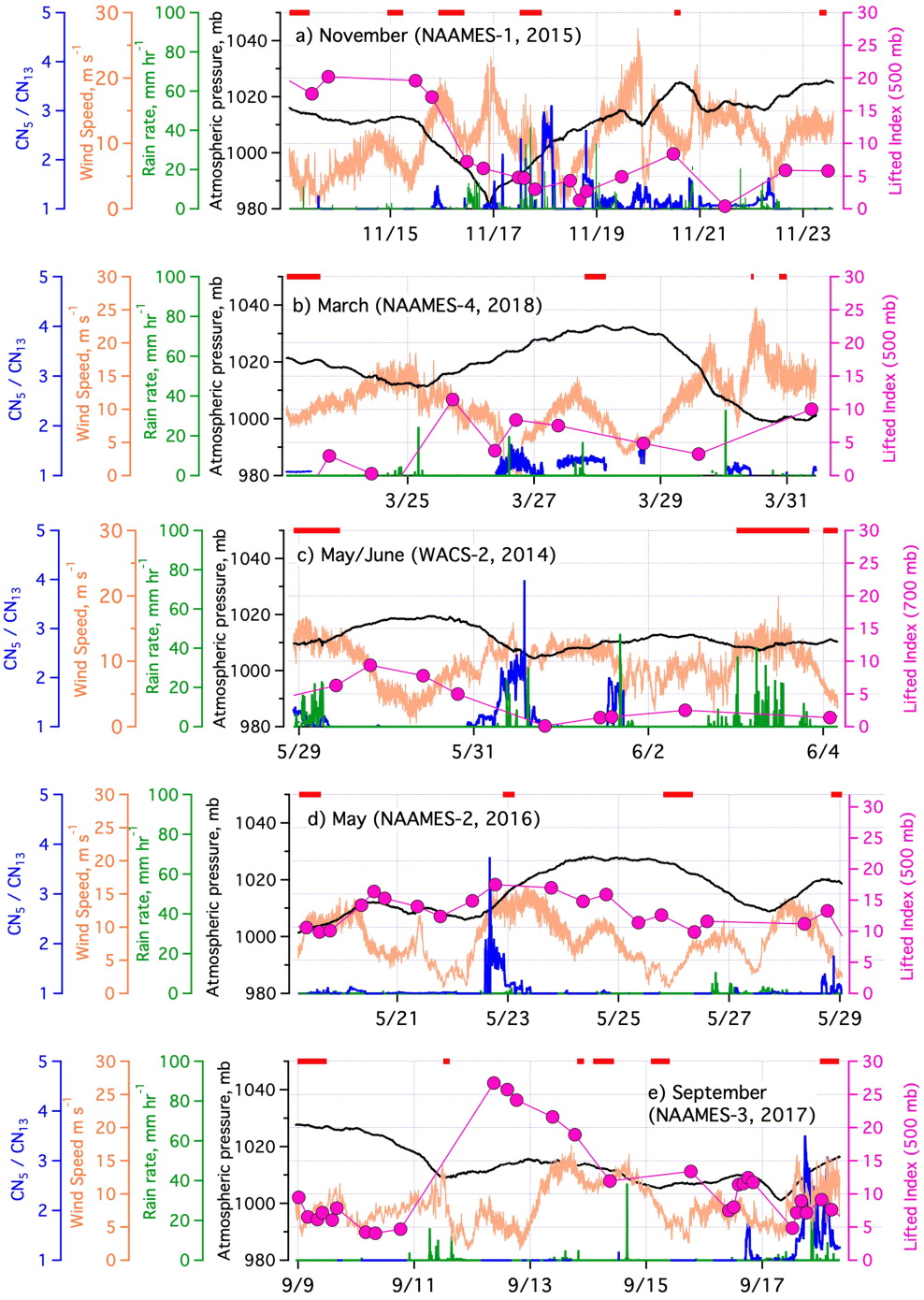

Figure 2. Ratio of the particle number concentration for D_p >5 nm divided by D_p >13 nm (CN_5/CN_{13}), wind speed, rain rate, atmospheric pressure, and Lifted Index for (a) November (NAAMES-1), (b) March (NAAMES-4), (c) May/June (WACS-2), (d) May (NAAMES-2), and (e) September (NAAMES-3). The clean marine times used in this analysis are indicated by red bars.

negative charge. Data were collected in 7 size bins from 0.2 to 0.8 μm D_{gn}. The Accumulation-DMPS operated with an aerosol flow rate of 0.5 L min^{-1} and a sheath air flow rate of 5 L min^{-1}. The aerosol was charged with a Po^{210} charge neutralizer upstream of each DMPS. Mobility distributions were collected every 5 min. The mobility distributions were inverted to a number distribution assuming a Fuchs-Boltzmann charge distribution from the Po^{210} charge neutralizer (Stratmann & Wiedensohler, 1997). The

overlapping channels between the two instruments were eliminated in the inversion. The data were corrected for diffusional losses and size-dependent counting efficiencies.

An Aerodynamic Particle Sizer (APS, TSI 3321) was located at the base of the mast inlet to minimize the loss of larger particles. The inlet to the APS was vertical. Its sample was drawn isokinetically from the larger flow to the DMPS. Number size distributions were collected with the APS every 5 min. The APS data were collected in 34 size bins with aerodynamic diameters ranging from 0.96 to 10.37 μm.

The DMPS and APS size distributions were merged by converting the APS data from aerodynamic to geometric diameters using calculated densities and associated water mass at the measurement RH based on the measured chemical composition (Quinn et al., 2002). The merged DMPS-APS size distributions were fitted with multiple lognormal modes using the lognormal fit function in IGOR Pro (Wavemetrics; Quinn et al., 2017). The first mode to be fit was in the largest diameter region of the size distribution, that is, the sea spray aerosol (SSA) mode. Two additional modes were then fit—an Aitken mode and an accumulation mode. No constraints were placed on the fit parameters of the modes. The ability of the multimodal fit to reproduce the measured size distribution was assessed with a chi-square test. Only cases where the chi-square value was less than the critical value at a significance level of 0.05 were included in the analysis.

2.5. CCN Activity

A DMT CCN Counter (CCNC) was used to determine CCN concentrations at supersaturations ranging from 0.1 to 0.3%. A multijet cascade impactor with a D_{aero} of 1.1 μm was upstream of the CCNC at the sampling RH described in section 2.1. The sampled air was dried prior to reaching the CCNC. As described in section 2.3 the CCNC sampled both heated (230 °C) and unheated aerosol. The CCNC was calibrated before, during, and after the experiments using methods described by Lance et al. (2006). The uncertainty associated with both the CCN number concentration and instrumental supersaturation was less than 10% (Lance et al., 2006; Roberts & Nenes, 2005).

The critical diameter for CCN activation, D_{crit}, was defined as the particle diameter at which

$$\frac{CCN_{measured}}{CNC_{integrated}} = 0.5 \tag{1}$$

where $CNC_{integrated}$, the integrated condensation nucleus concentration, was found by integrating from the largest diameter measured down to the diameter where the above equation was satisfied. Uncertainty in equation (1) and, therefore in D_{crit}, is estimated at ±20% based on a root sum of squares of the errors in the number concentrations derived from the CCN counter (±10%) and the measured size distributions (±18%). The actual uncertainty in D_{crit} will deviate from this estimate depending on the slope of the size distribution around D_{crit}, that is, whether D_{crit} is greater than or less than modal D_{gn}.

Kappa, κ, the hygroscopicity parameter, was calculated from the measurement supersaturation value (S_c) and D_{crit} using

$$\kappa = \frac{4A^3}{27D_{crit}^3 ln^2 S_c} \tag{2}$$

where

$$A = \frac{4\sigma M_w}{RT\rho_w}, \tag{3}$$

σ is the surface tension at the air-water interface of the particle set equal to 0.073 J m^{-2} and M_w and ρ_w are the molecular weight and density of water, respectively (Petters & Kreidenweis, 2007).

2.6. Aerosol Chemical Composition

Conductive silicone tubing was used to connect sampling tubes from the mast inlet to impactors used to collect aerosol for the analysis of inorganic ions. Stainless steel tubing was used for impactors that collected aerosol for organic carbon analysis. To prevent contamination, air flow through the impactors was controlled so that sampling took place only when the relative wind and number concentrations indicated that

the sample air was not affected by emissions from the ship's stack. Impactor sampling time periods ranged from less than an hour up to 18 hr.

2.6.1. Inorganic Ions

A two stage multijet cascade impactor (Berner et al., 1979; $D_{50,aero}$ of 0.18 and 1.1 μm at the RH values described in section 2.1) was used for the collection of aerosol for analysis of inorganic ions (Na^+, NH_4^+, $SO_4^=$, and Cl^-) and methanesulfonic acid (MSA). Ion concentrations were determined by ion chromatography (Quinn et al., 1998). Details of sample handling and blank determination can be found in Quinn et al. (2002). Non-sea salt (nss) sulfate concentrations were calculated by subtracting sea salt sulfate (based on measured Na^+ concentrations and the ratio of sulfate to sodium in seawater) from total measured sulfate. Sea salt concentrations were calculated as

$$\text{Sea salt } (\mu g\ m^{-3}) = Na^+(\mu g\ m^{-3}) \times 1.47 + Cl^-(\mu g\ m^{-3}) \quad (4)$$

where 1.47 is the seawater ratio of $(Na^+ + K^+ + Mg^{+2} + Ca^{+2} + SO_4^= + HCO_3^-)/Na^+$ (Holland, 1978). This approach prevents the inclusion of non-sea salt K^+, Mg^{+2}, Ca^{+2}, $SO_4^=$, and HCO_3^- in the sea salt mass and allows for the loss of Cl^- mass through Cl^- depletion processes (Quinn & Bates, 2005).

Sources of uncertainty in the ionic mass include the air volume sampled (±5%), the extract liquid volume (±3.3%), 2 times the standard deviation of the blank values measured over the course of the experiment, and the precision/calibration of the method (±5%). The average overall uncertainly was ±8.5%.

2.6.2. Organic Carbon

Precombusted (500°) quartz fiber filters were used to collect samples for the analysis of organic carbon (OC). Charcoal diffusion denuders were placed upstream of two single-stage impactors ($D_{50,aero}$ of 0.18 and 1.1 μm at the RH values described in section 2.1) to remove gas phase organic species. A quartz back filter downstream of the sample filter was used as a filter blank. OC concentrations were quantified with a Sunset Laboratory thermal-optical analyzer. Three temperature steps were used to evolve OC under O_2-free conditions (230, 600, and 870 °C). All OC was found to be removed at 600 °C or less indicating a lack of inorganic carbonates in the aerosol samples. OC concentrations were converted to total particulate organic matter (POM) using the factor of 2.0 recommended by Turpin and Lim (2001) for nonurban atmospheres. Based on the range of reported values, the uncertainty in the POM factor is ±31% (Turpin & Lim, 2001). Additional sources of uncertainty in the POM mass concentration include the air volume sampled (±5%) and the precision and calibration of the instrument (±5%; Schauer et al., 2003). The root sum of squares of these errors yields an overall uncertainty of ±33%.

2.7. Aerosol Light Absorption Coefficient

The absorption coefficient for submicron aerosol was measured by monitoring the change in transmission through a filter with a Particle Soot Absorption Photometer (PSAP; Radiance Research). The PSAP was downstream of a cascade impactor with a $D_{50,aero}$ of 1.1 μm (RH <30%). Measured values were corrected for a scattering artifact, the deposit spot size, the PSAP flow rate, and the manufacturer's calibration as per Bond et al. (1999). Values are reported at a wavelength of 550 nm, 0 °C, and 1,013 mb.

2.8. Sea Sweep Measurements

The Sea Sweep in situ SSA particle generator has been described previously in detail (Bates et al., 2012). Briefly, Sea Sweep was deployed off the port bow of the ship. It produced sea spray aerosol with a flow of compressed air through frits 0.75 m below the ocean surface. The freshly emitted SSA was distributed to all of the aerosol sampling equipment described above. Ambient aerosol was excluded from the Sea Sweep samples with a flow of particle free air that formed a curtain around Sea Sweep.

2.9. Atmospheric DMS

Atmospheric DMS was measured with an Atmospheric Pressure-Chemical Ionization Mass Spectrometer. An internal isotopic standard (triple deuterated DMS) was introduced at the tip of the inlet (located on the foremast of the ship) to characterize changes in inlet characteristics and instrument drift.

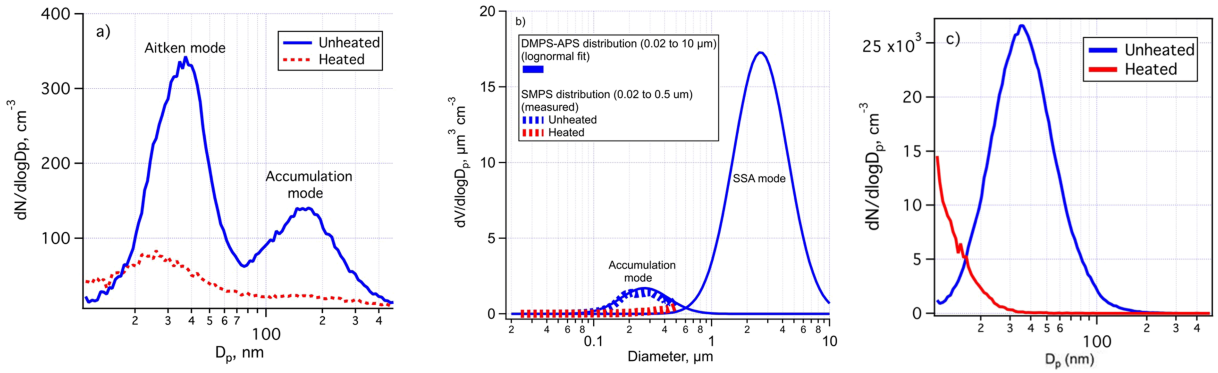

Figure 3. Unheated and heated ambient marine aerosol (a) number and (b) volume size distribution from WACS-2. The number size distribution was measured with an SMPS which covers the size range of 0.02 to 0.5 μm. Shown in (b) are the unheated and heated volume size distributions calculated from the SMPS number distributions and a lognormally fitted distribution from a differential mobility particle sizer (DMPS) which covers the range of 0.02 to 0.8 μm and an aerodynamic particle sizer (APS) which covers the range of 0.5 to 10 μm. The SMPS, DMPS, and APS data were measured simultaneously during WACS-2 (29 May 2014). The unheated and heated $(NH_4)_2SO_4$ calibration aerosol in (c) shows that particles reformed between the denuder and SMPS were less than 30 nm in diameter and made up less than 10% of the total particle number concentration.

2.10. Supporting Measurements

Wind speed and direction, atmospheric temperature and pressure, and relative humidity were based on an average of two Vaisala WXT520 sensors mounted on the bow tower (19.5 m above sea level). True wind speed and direction were calculated from the relative wind taking into account the ship's motion from the GPS and the ship's heading from the GPS compass. Rain rate was based on an average of Vaisala WXT520 and WXT536 sensors located near the top of the aerosol sampling mast (17 m above sea level). Rain rates measured at wind speeds greater than 15 m s^{-1} were omitted from the analysis as they may have been influenced by sea spray hitting the sensors.

Radon (^{222}Rn—half-life of 3.82 days) was measured using the method of Whittlestone and Zahorowski (1998). A photomultiplier counted the radon daughters produced in a 750-L decay tank for a 30-min period. The detector was standardized using radon emitted from a dry radon source (RN-25, Pylon Electronics Corp.). Background counts were measured under conditions of zero air flow.

Radiosondes were launched every 6 hr to measure vertical profiles of temperature, dew point, and wind speed and direction. The degree of atmospheric convective activity was estimated from the Lifted Index (LI) which was calculated from the radiosonde data (Bates et al., 1998; Galway, 1956). LI is equal to $T_{500} - T_L$ where T_{500} is the in situ temperature at 500 mb and T_L is the resultant temperature after a moist adiabatic lifting of an air parcel within the marine boundary layer (MBL) to 500 mb. Lower values indicate greater instability.

HYSPLIT back trajectories (Stein et al., 2015) were calculated for three arrival heights (100, 500, and 1,000 m) for the ship's position at 6-hr intervals using the Global Forecasting System 0.25-degree model.

3. Measurement Approach

Marine ambient aerosol is a complex mixture, in both microphysical and chemical terms, due to multiple sources, formation, and growth mechanisms. The Aitken mode (D_{gn} of ~0.01 to 0.1 μm at 60% RH) results primarily from entrainment of newly formed particles from the free troposphere (Clarke et al., 1998; Raes, 1995). Model simulations have shown that if wet scavenging removes preexisting aerosol, which reduces aerosol surface area, homogeneous nucleation of new particles can occur (Pirjola et al., 2000). Instances of particle nucleation in the MBL have been reported but are rare due to the large amount of surface area associated with SSA (Covert et al., 1992). For typical conditions in the remote, open ocean MBL (high SSA surface area concentrations and low concentrations of condensable vapors), boundary layer nucleation has little theoretical or observational basis (Quinn & Bates, 2011). The accumulation mode (D_{gn} of ~0.1 to 1.0 μm at 60% RH) results from the condensation of gas phase species onto Aitken mode particles, particle coagulation,

and cloud processing (Hoppel et al., 1994). Coarse mode particles (D_{gn} >~1 μm at 60% RH) are due to wind-driven bubble bursting at the ocean surface (Lewis & Schwartz, 2004; Monahan et al., 1983; Saltzman, 2009).

A combination of measurements of unheated and heated number size distributions, unheated and heated CCN concentrations, and aerosol composition was used to quantify and identify primary and secondary aerosol components in the MBL that could be related to the state of the phytoplankton bloom. Figure 3a shows examples of unheated and heated number size distributions measured with the SMPS over the 0.02- to 0.5-μm size range. The unheated size distribution yields the total number of particles in the Aitken and accumulation modes with an emphasis on volatile material, while the heated size distribution reveals the presence of nonvolatile material in the Aitken mode size range upon heating the aerosol to 230 °C. Although this material may have been present at larger particle sizes prior to heating, it is referred to throughout the paper as being in the Aitken mode size range upon heating to 230 °C to describe its size after heating. Measurements of unheated and heated CCN and CN concentrations were used to indirectly determine the composition and source of the nonvolatile material.

Figure 3b shows a lognormal fit of a volume size distribution measured with the combination of a DMPS and an APS. Overlaid are unheated and heated volume size distributions from the SMPS. The unheated size distribution yields the amount of volatile, secondary volume in the accumulation mode while the heated size distribution reveals the tailing of the nonvolatile SSA mode into the accumulation mode.

As discussed in section 2.3, unheated and heated size distributions were limited to particles larger than 0.03 μm because tests with ammonium sulfate aerosol showed that approximately 10% of particles smaller than 0.03 μm were a result of particle reformation between the thermal denuder and the SMPS. As shown in Figure 3c, the reformed particles had a "ski slope" size distribution with a modal diameter less than 0.03 μm. Removing them from the analysis is an effective approach for eliminating this artifact.

Chemical composition measured with ion chromatography and thermal-optical analysis of particles with $0.18 < D_{aero} < 1.1$ μm ($0.15 < D_{gn} < 0.95$ μm assuming $(NH_4)_2SO_4$ at 60% RH) was used to determine the composition of particles in the accumulation mode size range. Size segregated aerosol collected with the impactors results in a mixing of modes since size ranges of the modes can overlap. As can be seen in Figure 3b, the SSA mode tails into the accumulation mode resulting in the sub-1.1 μm minus sub-0.18 μm containing both the accumulation mode and SSA mode. Hence, we refer to the aerosol with $0.18 < D_{aero} < 1.1$ μm collected with the impactors as representing the "accumulation mode size range" rather than the actual mode.

Much of the data analysis was based on the chemical composition data from the impactor samples. Densities derived from the impactor data were used to merge the DMPS and APS size distributions. Impactor-based concentrations of volatile and nonvolatile POM were compared to the heated and unheated size distributions. Concentrations of sea salt, nss $SO_4^{=}$, NH_4^{+}, and POM (from the impactors) were regressed against CCN concentrations. Because of the heavy reliance on the impactor data, all data sets were averaged over the impactor samples collected during periods of clean marine air. These periods are indicated by the red bars shown in Figure 2 for each experiment.

4. Results

4.1. Ocean and Atmosphere Conditions During WACS-2 and NAAMES

Surface ocean and atmospheric conditions encountered during WACS-2 and the four NAAMES cruises are briefly described here in order of season/bloom phase (November (NAAMES-1), March (NAAMES-4), May/June (WACS-2 and NAAMES-2), September (NAAMES-3)). More detail about conditions and surface ocean measurements can be found in the NAAMES overview paper (Behrenfeld et al., 2019). Seasonal averages of wind speed, rain rate, radon, CN, and CCN (0.1% S) concentrations, aerosol light absorption coefficient, atmospheric DMS, and surface seawater chlorophyll for the time periods included in this analysis and indicated in Figure 2 are given in Table 1.

In the discussion below, a CN_5/CN_{13} ratio larger than 1 is attributed to downward mixing of particles from the free troposphere into the MBL. A regression of LI values calculated from radiosonde vertical profiles of temperature versus CN_5/CN_{13} over all experiments results in a coefficient of determination, r^2, of 0.51 providing evidence for this assumption (Figure 4a). LI versus the number concentration of nonvolatile particles

Table 1
Seasonal Averages and Standard Deviations for Meteorological, Aerosol, and Surface Seawater Parameters Measured During WACS-2 and the Four NAAMES Cruises During Clean, Marine Atmospheric Conditions as Defined by Radon, Particle Number Concentration (CN > 5 nm), Aerosol Light Absorption Coefficient, and HYSPLIT Back Trajectories

	November (NAAMES-1)	March (NAAMES-4)	May/June (WACS-2)	May/June (NAAMES-2)	September (NAAMES-3)
Wind speed (m s^{-1})	9.6 ± 3.8 (0.4, 20.0)	10.0 ± 2.9 (6.3, 23.0)	10.0 ± 5.0 (2.7, 20.0)	7.0 ± 4.0 (0.7, 15.0)	9.4 ± 2.5 (3.6, 16.0)
Rain rate (mm hr^{-1})	0.15 ± 1.50 (0.00, 42.00)	0.02 ± 0.23 (0.00, 7.60)	5.00 ± 4.00 (0.00, 140.00)	0.01 ± 0.12 (0.00, 2.90)	0.03 ± 0.34 (0.00, 9.20)
Radon (mBq m^{-3})	260 ± 140 (102, 520)	280 ± 180 (120, 510)	310 ± 75 (58, 352)	250 ± 90 (81, 420)	280 ± 78 (130, 440)
CN (cm^{-3})	77 ± 38 (13, 290)	380 ± 190 (89, 980)	360 ± 140 (88, 500)	410 ± 140 (140, 1000)	270 ± 180 (114, 750)
Light absorption coefficient (Mm^{-1})	0.04 ± 0.01 (BC = 15 ng m^{-3})	0.16 ± 0.13 (BC = 21 ng m^{-3})	0.12 ± 0.05 BC = 16 ng m^{-3}	0.19 ± 0.19 BC = 25 ng m^{-3}	0.11 ± 0.09 BC = 15 ng m^{-3}
CCN at 0.1% S (cm^{-3})	16 ± 11	82 ± 24	81 ± 17	85 ± 52	75 ± 45
Atmospheric DMS (pptv)	67 ± 7 (55, 86)	140 ± 36 (36, 190)	Not available	311 ± 300 (19, 960)	100 ± 66 (20, 270)
Chlorophyll (mg m^{-3})	0.30 ± 0.21 (0.13, 1.00)	0.71 ± 0.24 (0.26, 1.40)	0.37 ± 0.18 (0.05, 0.97)	1.60 ± 1.20 (0.55, 5.30)	0.57 ± 0.18 (0.19, 0.83)

Note. Numbers in parentheses are minimum and maximum values except for the light absorption coefficient where black carbon (BC) concentrations are reported based on the absorption coefficient and a mass absorption coefficient of 7.5 m^2 g^{-1} (Bond et al., 2013).

yields an r^2 of 0.41 indicating an upper atmosphere source of particles found in the Aitken mode size range after heating to 230 °C (Figure 4b).

NAAMES-1 (November) targeted the early winter transition event initiating the annual phytoplankton blooming phase. The clean marine aerosol periods for NAAMES-1 occurred between 13 and 23 November 2015. Initially, wind speeds were relatively low (<10 m s^{-1}) and rainfall was relatively infrequent (Figure 2a). Based on LI values, the MBL was well-defined and stable (Figure 2a). A low-pressure system moved through the region late on 16 November resulting in higher wind speeds, sea states, and frequent rainfall. These conditions persisted throughout the end of the clean marine sampling period along with lower LI values indicating atmospheric instability. Back trajectories indicated that the predominant air flow was from the Canadian Arctic with the transport of air from up to 3,500-m altitude into the MBL. CN_5/CN_{13} ratios often exceeded 1 indicating downward mixing of newly formed particles from the free troposphere into the MBL due to atmospheric instability. Ocean mixed layer depths exceeded 100 m along the cruise track. Chlorophyll concentrations were low, with a mean value of 0.3 mg m^{-3} (Table 1). In general,

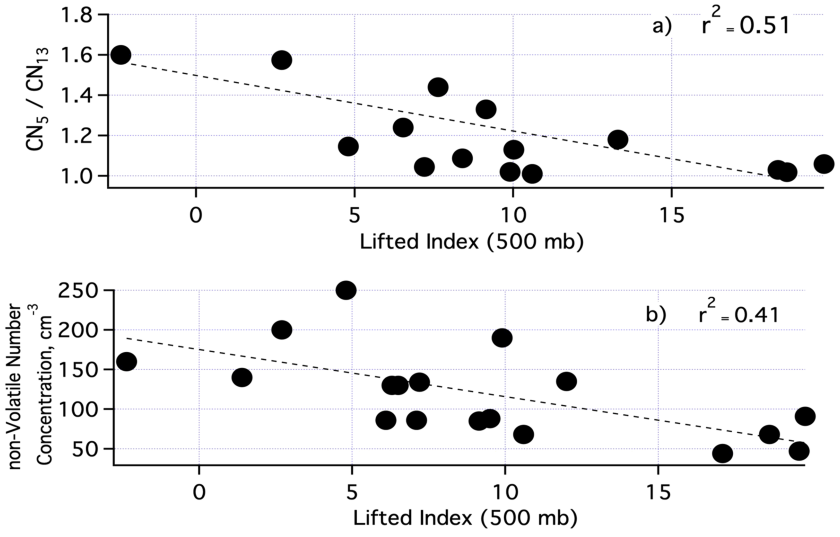

Figure 4. Lifted Index (LI) for 500 mb versus (a) CN_5/CN_{13} and (b) nonvolatile number concentration for NAAMES-1, NAAMES-2, NAAMES-3, NAAMES-4, and WACS-2.

phytoplankton cell concentrations were low compared to other NAAMES cruises but the plankton communities were taxonomically diverse and dominated by cyanobacteria and picoeukaryotes. Normalized variable fluorescence indicated low levels of phytoplankton physiological stress. Atmospheric DMS concentrations in the MBL were low, ranging from ~50 to 90 pptv.

The NAAMES-4 cruise in March and April was focused on the accumulation phase of the annual phytoplankton cycle. Clean marine periods for NAAMES-4 occurred between 23 and 30 March 2018. NAAMES-4 covered more southern latitudes than the other cruises since it left from San Juan, Puerto Rico instead of Woods Hole, MA. It also only went to 44.5°N due to weather conditions (compared to the 53° to 56°N range of the other cruises). Once the ship reached 39°N, clean marine conditions were confined to the easternmost portion of the cruise track (east of 45°W) due to air masses coming off of the eastern United States along the western portion of the cruise track. The origin of the air masses varied between the southern North Atlantic and northern Canada, with transport of air from altitudes up to 8,000 m into the MBL. With the exception of the last two days of this period, winds were calmer than those observed during November (Figure 2b). In addition, rainfall was less frequent. Measurements of CN_5/CN_{13} were limited due to malfunctioning CN counters. However, periods with data include ratios larger than 1, indicating the presence of newly formed particles. Low LI values (Figure 2b) suggest a free troposphere source of these particles due to atmospheric instability. During clean marine periods, chlorophyll was highly variable, with concentrations ranging from 0.26 to 1.4 mg m^{-3}. Phytoplankton community composition was also highly variable and predominantly composed of small cells with patches of large diatoms occurring sporadically. Both an "accumulation" phase of the bloom and stressed phytoplankton communities were encountered. Atmospheric DMS concentrations varied between 36 and 190 pptv.

WACS-2 was conducted in May with clean marine periods occurring between 28 May and 4 June 2014. Frontal passages moved through the study region on 29 May, 31 May, and 3 June with corresponding higher wind speeds and rain rates (Figure 2c). Air mass flow was from the Labrador Sea via the Canadian Arctic, with transport of air from altitudes of 3,500 m into the MBL. CN_5/CN_{13} ratios were elevated in association with the 29 and 31 May frontal passages. Data were not available for the 3 June storm. Low LI values indicate a free troposphere source of aerosol into the MBL (Figure 2c). Surface ocean measurements were more limited than during NAAMES. Chlorophyll concentrations were low (<0.5 mg m^{-3}).

NAAMES-2 was conducted in May and June and targeted the annual bloom climax period. Clean marine aerosol periods during NAAMES-2 occurred between 19 and 29 May 2016. Lower wind speeds (Figure 2d) and sea states prevailed during May/June compared to November and March with the exception of two storms that passed through the region on 22 and 23 May and 28 and 29 May. Rain was infrequent throughout. Similar to NAAMES-1, air mass flow was from the Canadian Arctic via the Labrador Sea but with fewer indications of transport from aloft based on back trajectories and LI values (Figure 2d). However, CN_5/CN_{13} ratios were elevated during the two storm periods. With the exception of the storm periods, ocean mixed layer depths ranged from 20 to 60 m. Chlorophyll concentrations were the highest observed across all cruises with values ranging from 0.55 to 5.3 mg m^{-3}. Phytoplankton biomass was dominated by cells less than 20 μm in diameter, with a greater contribution from picoeukaryotic and nanoeukaryotic phytoplankton than in November. Physiological stress levels were low. MBL atmospheric DMS concentrations were the highest observed for all cruises, with concentrations ranging from 19 to 960 pptv.

NAAMES-3 occurred during the declining phase of the phytoplankton annual cycle. Clean marine aerosol periods for NAAMES-3 occurred between 8 and 18 September 2017. Higher winds and lower atmospheric pressure associated with hurricane Jose were encountered on 17 and 18 September (Figure 2e). CN_5/CN_{13} was significantly elevated during this period, indicating downward mixing of newly formed particles from the free troposphere. Throughout the sampling period, back trajectories indicated flow from the Canadian Arctic and the North Atlantic with indications of transport from between 1,000- to 9,000-m altitude to the surface. LI index values at the beginning and end of the sampling period were relatively low, indicating atmospheric instability (Figure 2e). Ocean mixed layer depths ranged from about 10 to 40 m. Chlorophyll concentrations were low (<0.6 mg m^{-3}). Phytoplankton communities were dominated by smaller cells and composed of *Synechococcus*, dinoflagellates, and other small (pico- and nano-) eukaryotic cells. The lowest normalized variable fluorescence values were measured during NAAMES-3, indicating a declining

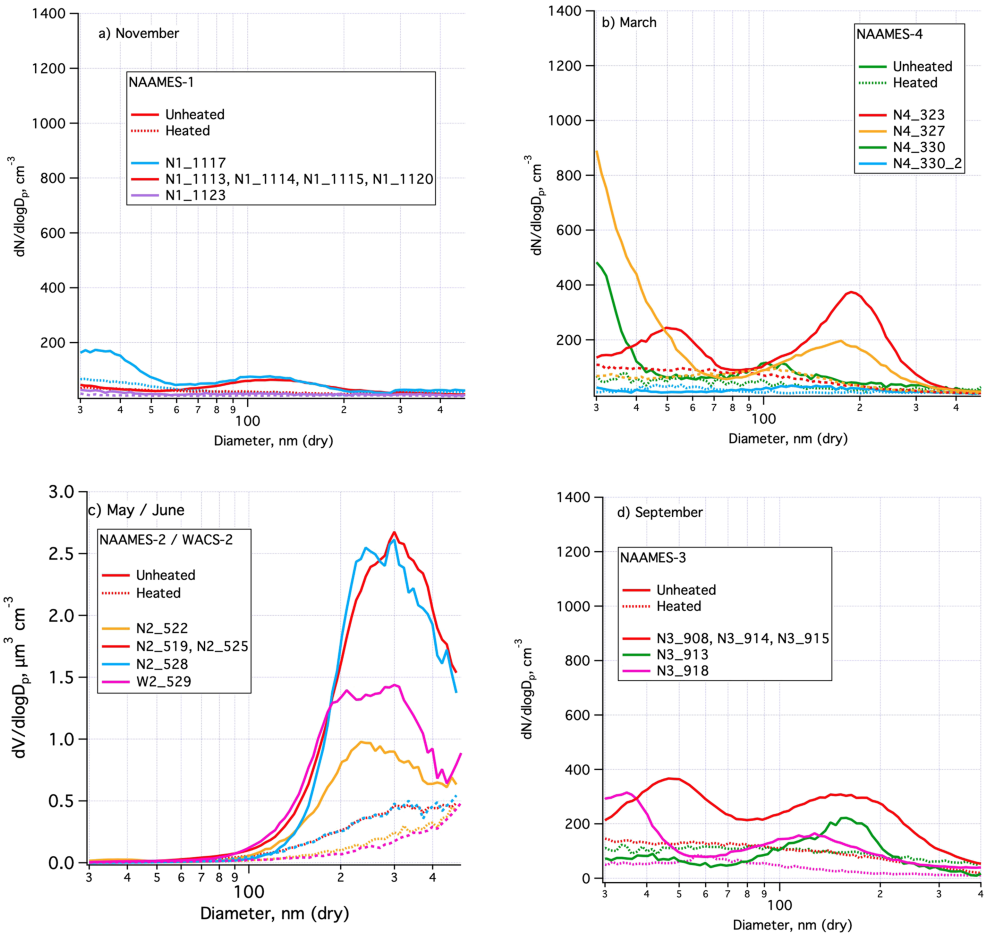

Figure 5. Unheated and heated number size distributions for (a) November (NAAMES-1), (b) March (NAAMES-4), (c) May/June (NAAMES-2 and WACS-2), and (d) September (NAAMES-3). Legend indicates cruise and date of sample. Samples with similar distributions are presented as averages for simplicity.

phytoplankton community experiencing physiological stress and declining in biomass. Atmospheric DMS concentrations ranged from 20 to 270 pptv.

4.2. Source, Composition, and Seasonality of Marine Aitken Mode Aerosol in the Western North Atlantic

Unheated and heated number size distributions for the four seasons are shown in Figure 5. In general, size distributions were bimodal with pronounced Aitken and accumulation modes as is typical of clean marine aerosol (Bates et al., 2002; Heintzenberg et al., 2000; Yoon et al., 2007). Seasonally averaged total number concentrations were lowest (77 ± 38 cm^{-3}) during November due to the Arctic source of the aerosol and frequent rain (Figure 6a and Table 1). The low number concentrations and associated meteorological conditions are similar to those reported for the eastern North Atlantic (Pennypacker & Wood, 2017). Average total number concentrations were similar for March, May/June, and September ranging from 270 to 410 cm^{-3}.

The fraction of the total number of particles in the Aitken, accumulation, and SSA modes was determined from a lognormal fit to the number size distributions measured with the DMPS and APS (see section 2.4). The number fraction of SSA mode particles was similar to those in the Aitken and accumulation modes during November (Figure 6b). During the other three seasons, the number fraction of SSA was less than 20%, which indicates a limited role for SSA as CCN except, perhaps, for low supersaturation conditions. Aitken mode number fractions were highest for March and September. Based on calculated back trajectories and

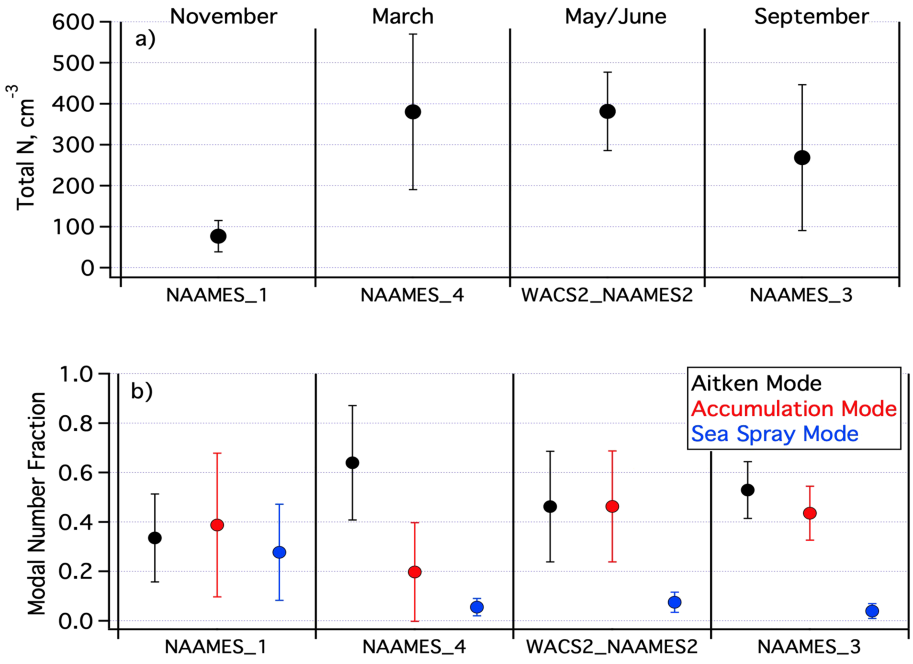

Figure 6. Seasonal average and standard deviation of (a) total measured number concentration and (b) the fraction of the total number in the Aitken, accumulation, and SSA modes. Average and standard deviations for each experiment were calculated over the impactor samples collected during the clean marine times shown in Figure 2 (red bars; four samples each for NAAMES-1, NAAMES-4, WACS-2, and NAAMES-2 combined; three samples for NAAMES-3).

LI values, the Aitken mode during March and September was likely due to recent downward mixing of air from the free troposphere (Figures 2b and 2e). Aitken and accumulation mode number fractions were similar for May/June and September.

During all seasons, number size distributions revealed the presence of refractory material in the Aitken mode size range after heating the aerosol to 230 °C. The nonvolatile number fraction, $NVol_{NF}$, was calculated from

$$NVol_{NF} = 1 - \frac{(Unheated\ number - Heated\ number)}{Unheated\ number} \quad (5)$$

where the unheated and heated number concentrations were integrated over number size distributions for D_{gn} greater than 0.03 μm. Average values of $NVol_{NF}$ were highest for November (0.62), in agreement with a relatively large SSA mode tailing into smaller size ranges and high wind speeds (Figure 7). Average values for March, May/June, and September were similar, ranging from 0.32 to 0.41.

Identifying and quantifying chemical species that occur in the Aitken mode is difficult due to small mass concentrations in this size range. In lieu of direct chemical measurements, the composition of refractory material in the Aitken mode after heating to 230 °C was probed with measurements of the CCN activity of heated sub-1.1-μm aerosol. Heating the bulk sub-1.1-μm aerosol leaves the Aitken mode shown in the heated number size distributions of Figure 5. That aerosol was subsequently sampled by the CCN instrument. A combination of the CCN measurements and particle number size distributions was used to estimate critical diameters, D_{crit}, for clean marine unheated and heated ambient aerosol (section 2.5). These values are compared with those of monodisperse SSA (D_{gn} = 50 nm, dry) generated by Sea Sweep during NAAMES-1, NAAMES-2, and NAAMES-3. NAAMES-4 data were not available for comparison. D_{crit} of both the unheated and heated ambient aerosol is significantly higher than Sea Sweep SSA by a factor of 2.4 to 5.2 at ~0.3% supersaturation (Table 2). These results indicate that, at least in terms of CCN activity, the nonvolatile material that resides in the Aitken mode after heating the aerosol to 230 °C is not related to sea spray aerosol.

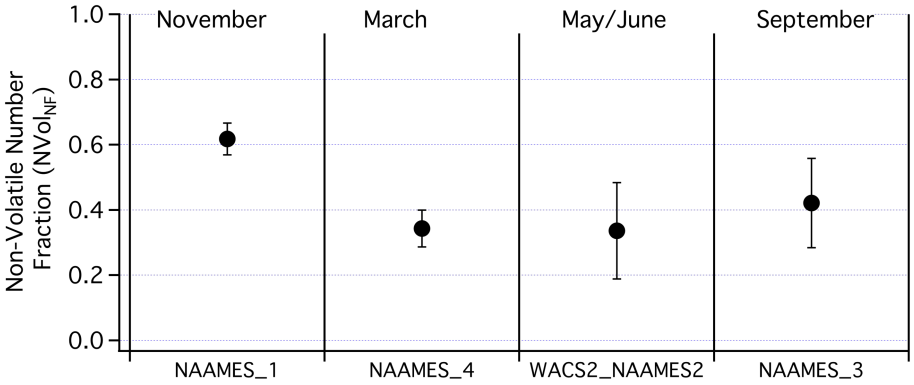

Figure 7. Average and standard deviation of the nonvolatile number fractions, $NVol_{NF}$, based on integrated number from the unheated and heated number size distributions over four seasons and equation 5. Average and standard deviations for each experiment were calculated over the impactor samples collected during the clean marine times shown in Figure 2 (red bars; four samples each for NAAMES-1, NAAMES-4, WACS-2, and NAAMES-2 combined; three samples for NAAMES-3).

The shape and size of the heated Aitken mode also indicate a non-SSA source. Both open-ocean and laboratory measurements indicate that SSA exists as a single mode with a modal diameter between 0.1 to 0.4 μm (Lewis & Schwartz, 2004; Modini et al., 2015; Prather et al., 2013; Quinn et al., 2017). If Sea Sweep generated SSA is sampled at an RH of 60% or lower and then heated to 230°, the difference between the unheated and heated number size distributions is within measurement uncertainties (Bates et al., 2012), indicating that it is unlikely that the nonvolatile material left in the Aitken mode size range after heating to 230 °C is SSA. Even for aged SSA that has existed in the atmosphere for hours to days and has undergone photochemical processing and reacted with atmospheric gas phase species, it is difficult to invoke a mechanism whereby the modal diameter would be reduced over time by a factor of 2 to 5. Given the atmospheric instability related to frontal passages during all seasons of NAAMES and the correlation of LI and the number concentration of nonvolatile particles shown in Figure 4 ($r^2 = 0.41$), it is more likely that the nonvolatile material is a result of downward mixing of particles from the free troposphere.

4.3. Source, Composition, and Seasonality of Marine Accumulation Mode Aerosol in the Western North Atlantic

Unheated and heated volume size distributions for November, March, May/June, and September are shown in Figure 8. During November, unheated and heated volume size distributions were similar, indicating a dominance by the SSA mode tailing into the accumulation mode and very little volatile material (Figure 8a). During March, half of the unheated and heated volume size distributions (Figure 8b) were similar to those measured during November indicating SSA with little volatile accumulation mode. In the other half, a pronounced volatile accumulation mode was observed in the unheated volume size distributions which, when heated, left behind a SSA mode. A volatile accumulation mode was observed in all of the

Table 2
Critical Diameters, D_{crit}, for Freshly Emitted SSA Generated From Sea Sweep and for Unheated and Heated (230°) Ambient Aerosol Measured During NAAMES-1, NAAMES-2, and NAAMES-3 at the Listed Critical Supersaturations, S_c

		Sea Sweep SSA	Ambient aerosol unheated	Ambient aerosol heated (230°)
Month/experiment	S_c (%)	D_{crit} (μm)	D_{crit} (μm)	D_{crit} (μm)
November NAAMES-1	0.31	0.05	0.15	0.21
March NAAMES-4	0.30		0.13	0.12
May/June NAAMES-2	0.28	0.05	0.17	0.15
September NAAMES-3	0.29	0.05	0.14	0.12

Note. Sea Sweep SSA values are based on monodispersed 50-nm particles. Sea Sweep data were not available for NAAMES-4. Data in the table are taken from Figure 13.

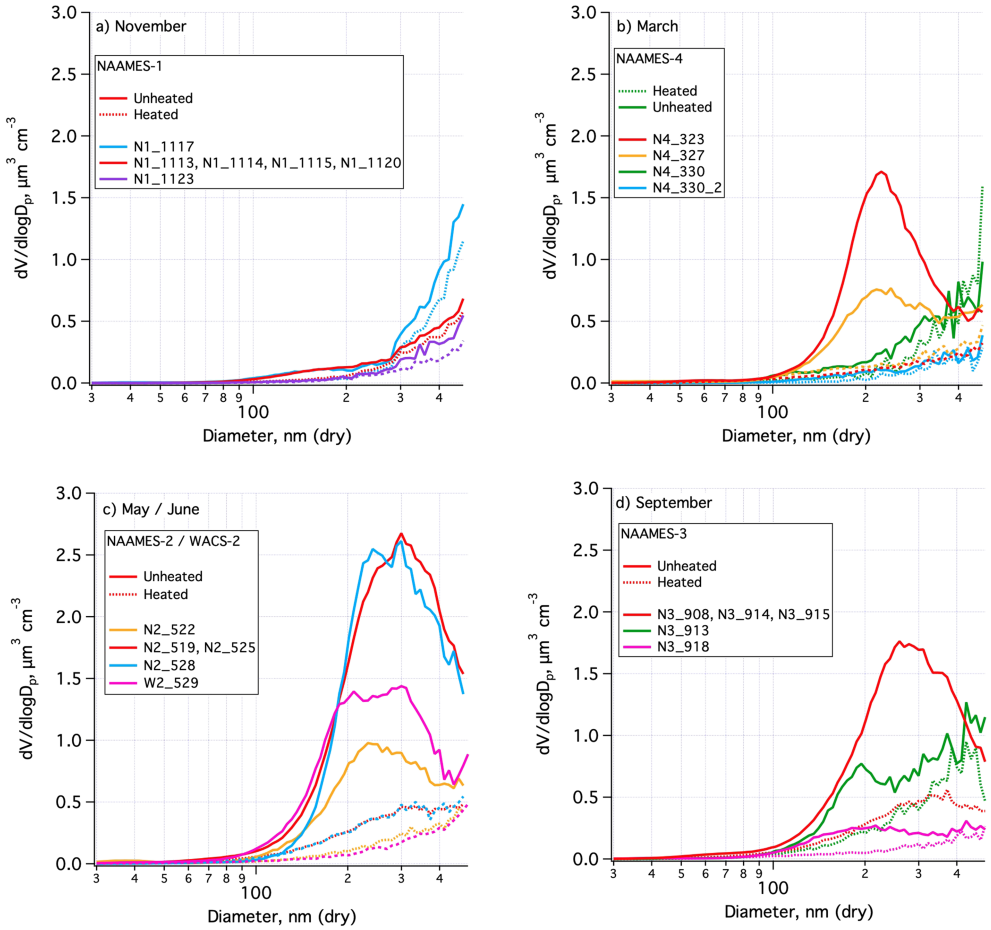

Figure 8. Unheated and heated volume size distributions for (a) November (NAAMES-1), (b) March (NAAMES-4), (c) May/June (NAAMES-2 and WACS-2), and (d) September (NAAMES-3). Legend indicates cruise and date of sample. Samples with similar distributions are presented as averages for simplicity.

May/June unheated volume size distributions (Figure 8c). In addition, these distributions included the largest volatile volume concentrations across all seasons. September was similar to March with a mix of a small to dominant volatile accumulation mode (Figure 8d).

The fraction of volatile volume, Vol_{VF}, for each season was calculated from

$$Vol_{VF} = \frac{(Unheated\ volume - Heated\ volume)}{Unheated\ volume} \quad (6)$$

where the unheated and heated volume concentrations were integrated over the size distributions shown in Figure 8 for each season. Vol_{VF} are lowest for November when wind speeds (up to 20 m s^{-1}) and rain rates (up to 42 mm hr^{-1}) were high (Figure 9). Vol_{VF} were highest during May/June corresponding to relatively low wind speeds and rain rates. Intermediate values of Vol_{VF} were observed in March and September.

Direct chemical measurements of particles with $0.18 < D_{aero} < 1.1$ μm ($0.15 < D_{gn} < 0.95$ μm) yield information about the composition of the volatile and nonvolatile components in the accumulation mode size range. Figure 10a shows the total mass concentration in the accumulation mode size range based on the sum of measured sea salt, nss $SO_4^=$ plus NH_4^+, and POM. Average concentrations are highest for November and slightly lower but similar for the other three months. The average mass fraction in the accumulation mode size range of each chemical component is shown in Figure 10b. Sea salt (based on equation 4) makes a significant contribution to the mass in the accumulation mode size range in all seasons but more so in November, contributing to the seasonally high accumulation mode size range mass and low V_{VF}. The

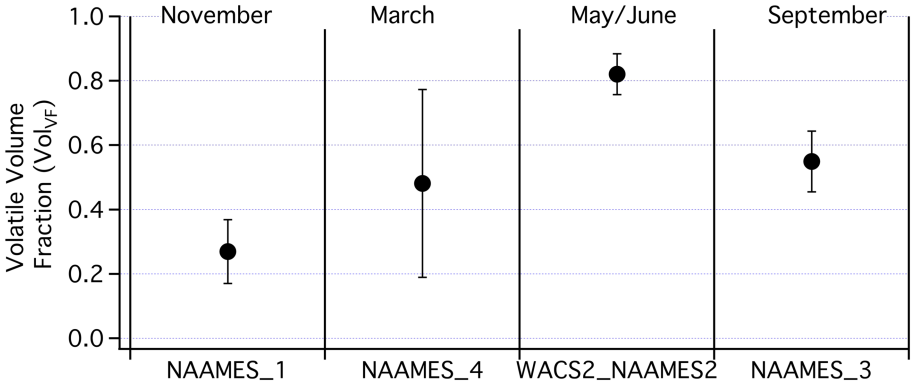

Figure 9. Average and standard deviation of the volume volatile fractions (Vol_{VF}) based on integrated volume from the unheated and heated volume size distributions over four seasons and equation 6. Average and standard deviations for each experiment were calculated over the impactor samples collected during the clean marine times shown in Figure 2 (red bars; four samples each for NAAMES-1, NAAMES-4, WACS-2, and NAAMES-2 combined; three samples for NAAMES-3).

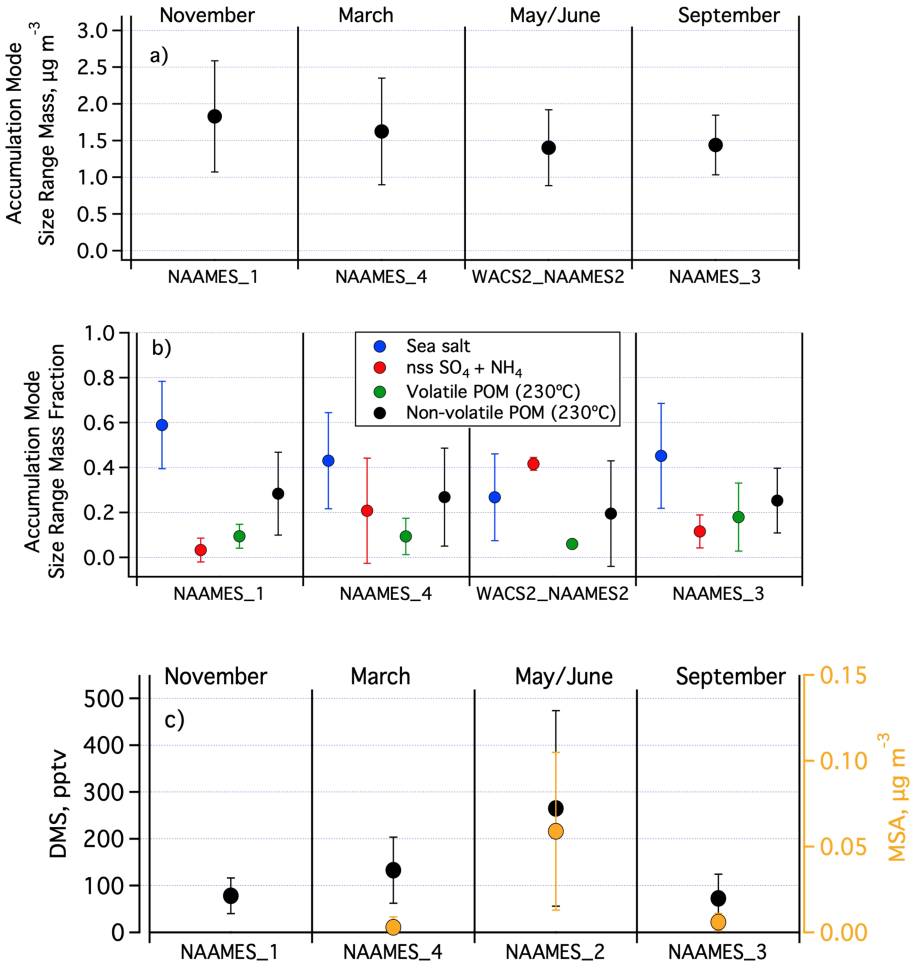

Figure 10. Average and standard deviation of accumulation mode size range values of (a) total mass concentration based on a sum of measured sea salt, nss $SO_4^=$ plus NH_4^+, and POM concentrations; (b) mass fractions of the chemical components; and (c) atmospheric DMS and MSA concentrations. Average and standard deviations for each experiment were calculated over the impactor samples collected during the clean marine times shown in Figure 2 (red bars; four samples each for NAAMES-1, NAAMES-4, WACS-2, and NAAMES-2 combined; three samples for NAAMES-3). No MSA data were available for NAAMES-1.

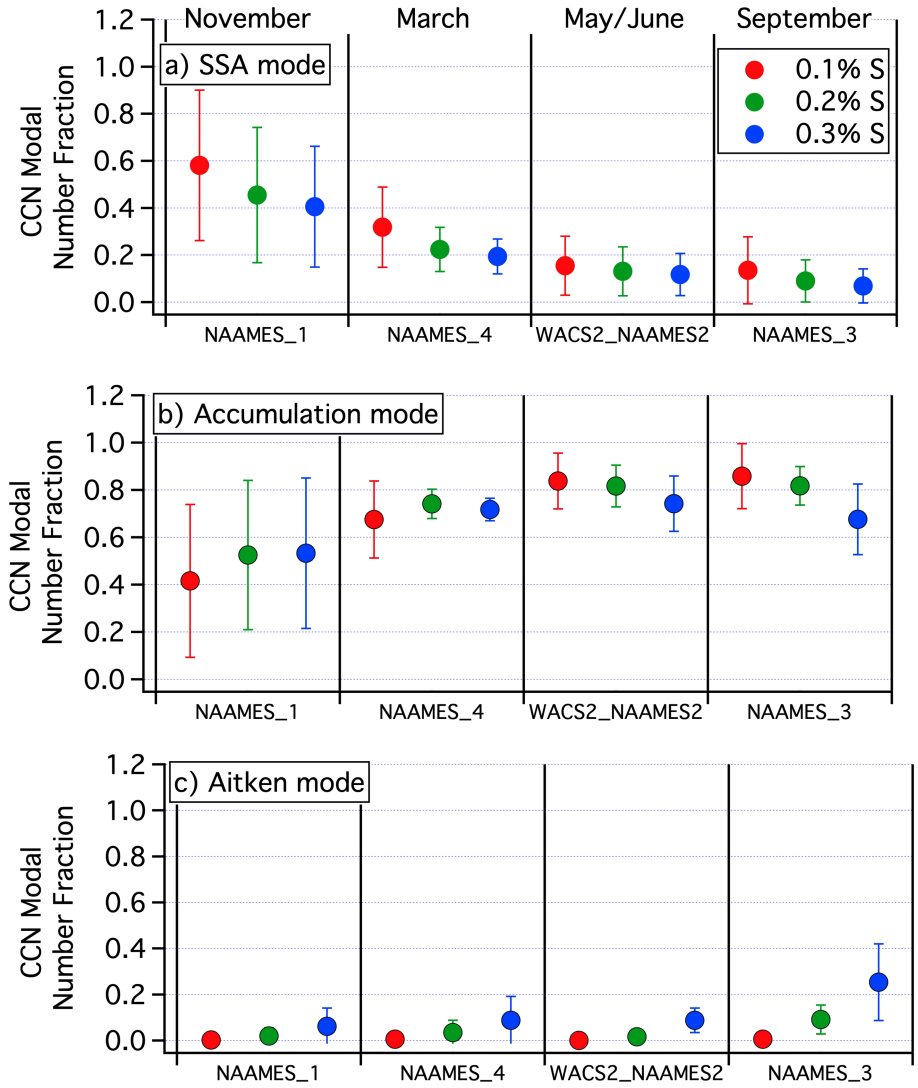

Figure 11. Average and standard deviation of the fraction of the total number of CCN in the (a) SSA, (b) accumulation, and (c) Aitken modes for November (NAAMES-1), March (NAAMES-4), May–June (WACS-2 and NAAMES-2), and September (NAAMES-3). Values are shown for 0.1, 0.2, and 0.3% supersaturation. Average and standard deviations for each experiment were calculated over the impactor samples collected during the clean marine times shown in Figure 2 (red bars; four samples each for NAAMES-1, NAAMES-4, WACS-2, and NAAMES-2 combined; three samples for NAAMES-3).

high sea salt concentrations are a result of the tailing of the SSA mode into the accumulation mode size range.

Average values of nonvolatile POM mass fractions are similar across seasons and at least a factor of 2 higher than the volatile POM mass fractions. Nss $SO_4^=$ plus NH_4^+ mass fractions are low with the exception of May/June, when average values are greater than either sea salt or POM. The seasonal pattern in the mass fraction of nss $SO_4^=$ corresponds to that of MSA, whose only source is the oxidation of DMS, and atmospheric DMS concentrations (Figure 10c), indicating that the large volatile fraction of the aerosol in the MBL during May/June was, in large part, a result of the oxidation of DMS. This result is not unexpected. For example, Andreae et al. (2003) reported that the evolution of the plankton bloom during spring in the North Atlantic affected the abundance of seawater and atmospheric DMS and nss $SO_4^=$ aerosol. Although this is not a new result, it is reported here as an identified link between the bloom state and marine aerosol for the western North Atlantic and addresses a primary objective of NAAMES.

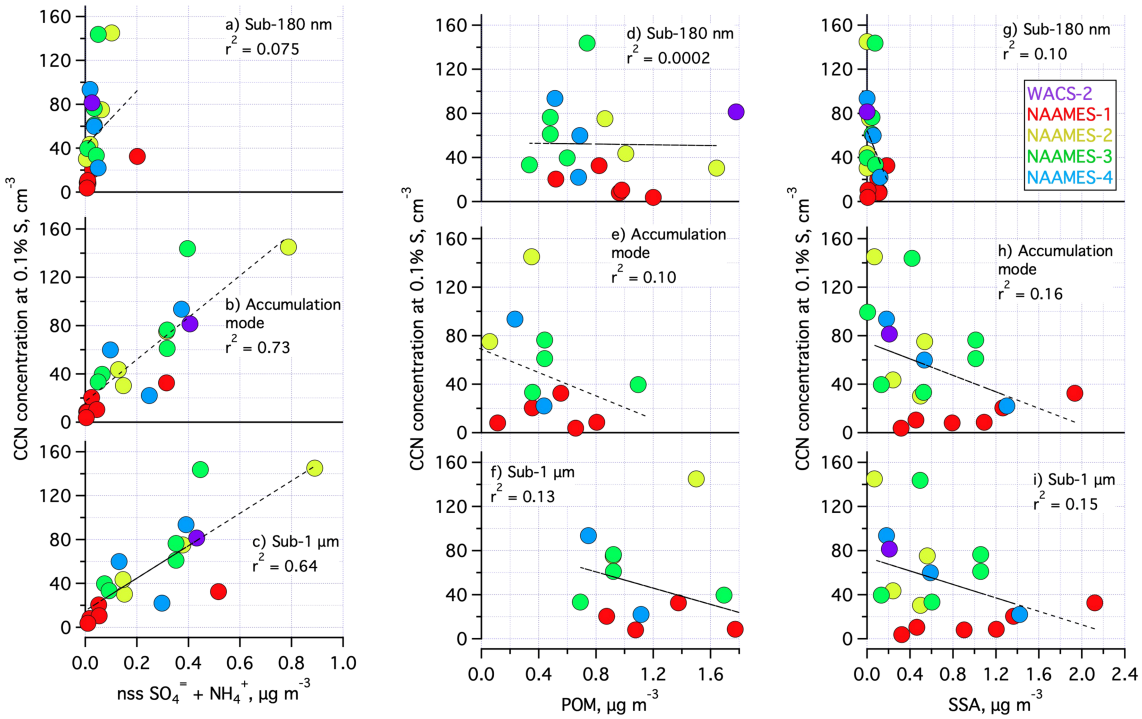

Figure 12. Linear regression of nss $SO_4^=$ + NH_4^+ versus CCN concentration (at 0.1% S) for the (a) sub-180-nm size range (D_{aero} < 0.18 µm), (b) accumulation mode (0.18 µm < D_{aero} < 1.1 µm), and (c) sub-1-µm size range; total POM versus CCN concentration for the (d) sub-180-nm size range, (e) accumulation mode, and (f) sub-1-µm size range; and SSA versus CCN concentration for the (g) sub-180-nm size range, (h) accumulation mode, and (i) sub-1-µm size range. Points are color coded by experiment.

4.4. Sources of CCN and Seasonal CCN Activity in the Western North Atlantic

The number of particles able to nucleate and form cloud droplets at a given supersaturation depends on total particle number concentration, size distribution, and chemical composition.

Using lognormal modes fit to measured number size distributions (section 2.4) and an assumed chemical composition, modal critical diameters, $D_{crit,modal}$, were calculated for the Aitken, accumulation, and SSA modes (Quinn et al., 2017). The number of CCN in each mode was then calculated based on $D_{crit,modal}$ and the corresponding lognormal mode size distribution. The Aitken and accumulation modes were assumed to be composed of a mixture of NH_4HSO_4 and POM based on the relative fractions of those two components in the sub-0.18- and sub-1.1 minus sub-0.18-µm impactor stages, respectively. POM was assumed to be water insoluble. The SSA mode was assumed to be pure NaCl.

The fraction of the total CCN number attributable to the SSA mode was highest for November (Figure 11a), which corresponds with November having a large SSA modal number fraction compared to the other seasons. At 0.1% supersaturation (S), the average value of the SSA mode CCN number fraction was around 0.6, compared to 0.4 for the accumulation mode (Figure 11b). For March, May/June, and September, the SSA CCN number fraction was considerably less, with average values of 0.31, 0.15, and 0.14, respectively, corresponding to the low SSA modal number fractions shown in Figure 6b. The accumulation mode made up the majority of the CCN at all supersaturations for March, May/June, and September. The CCN number fraction was largest for the Aitken mode during September at 0.3% S.

CCN concentrations measured at 0.1% S were regressed against concentrations of nss $SO_4^=$ plus NH_4^+, total POM, and sea salt to further assess sources of CCN to the western North Atlantic MBL. Data from all cruises were combined to increase the robustness of the correlations. CCN concentrations at 0.1% S were used because this supersaturation had the most data available over all cruises. Regressions were performed for the sub-0.18-, sub-1.1 minus sub-0.18-µm, and sub-1.1-µm size fractions (Figure 12).

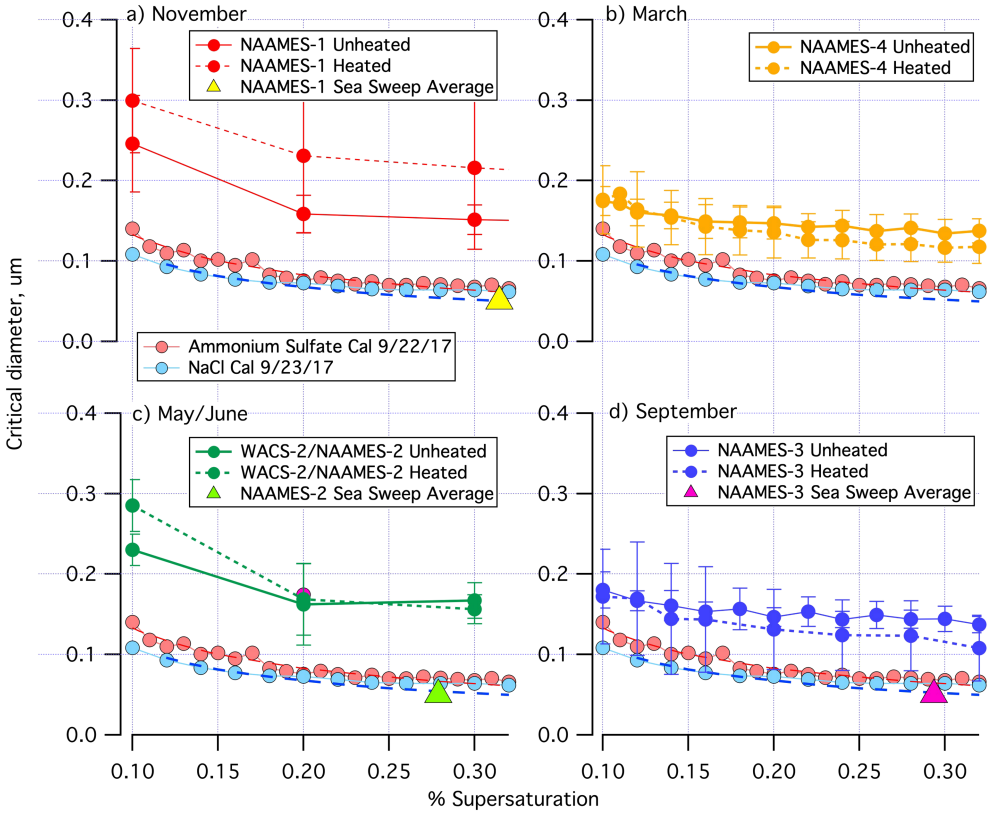

Figure 13. Critical diameters as a function of supersaturation averaged over all clean marine time periods for (a) November (NAAMES-1), (b) March (NAAMES-4), (c) May/June (WACS-2/NAAMES-2), and (d) September (NAAMES-3). Unheated CCN measurements are shown as solid lines while heated are dashed lines. Critical diameters for calibration aerosol ($(NH_4)_2SO_4$ and NaCl) are shown for reference. Long dashed lines under the calibration curves are calculated from Köhler theory (Seinfeld & Pandis, 2006). Also shown are results for monodisperse SSA (D_{gn} = 50 nm, dry) freshly generated by Sea Sweep averaged over each cruise.

CCN concentrations versus nss $SO_4^=$ + NH_4^+ in the accumulation mode size range had the highest coefficient of determination of all three chemical components (r^2 = 0.73), indicating that nss $SO_4^=$ aerosol was the major contributor to the MBL CCN population. With all of the experiments combined, POM and SSA were not significantly correlated with CCN for any size range. Considering NAAMES-1 by itself, however, yielded an r^2 value of 0.83 for accumulation mode size range SSA versus CCN concentration (Figure 12h). SSA was only significantly correlated with CCN when nss $SO_4^=$ was low in concentration due to the lack of phytoplankton-derived DMS in November.

A combination of CCN measurements of sub-1.1-μm polydisperse aerosol and particle number size distributions was used to estimate critical diameters, D_{crit}, and the hygroscopicity parameter kappa, κ, for clean marine ambient aerosol during the four different seasons of WACS-2 and NAAMES (section 2.5). More emphasis is put on the D_{crit} values than κ given the large uncertainties in the calculation of κ due to propagation of errors through D_{crit}^3 and $\%S^2$. D_{crit} averaged over each season for 0.1 to 0.3% S are shown in Figure 13. For reference, D_{crit} of calibration aerosol ($(NH_4)_2SO_4$ and NaCl) are shown as well as seasonally averaged values for freshly emitted SSA generated using Sea Sweep during the NAAMES cruises. D_{crit} of unheated ambient aerosol varied between seasons. The highest average value, 0.25 ± 0.06 μm at 0.1% S, occurred in November and corresponded to a kappa of 0.11 ± 0.05. High D_{crit} values of 0.23 ± 0.02 μm at 0.1% S were also found for May/June, corresponding to a kappa of 0.12 ± 0.02. Lower D_{crit} values were observed in March (0.17 ± 0.02 at 1% S) and September (0.18 ± 0.02 at 1% S) and corresponded to average kappa values of 0.21 ± 0.05 and 0.25 ± 0.08, respectively. In all seasons, D_{crit} values were higher than $(NH_4)_2SO_4$, NaCl, and freshly emitted SSA, indicating an internal mixture of $SO_4^=$ (κ = 0.61), SSA (κ = 1.2 to 1.4 based on

Sea Sweep SSA during NAAMES-1, -2, and -3), and organics ($\kappa = 0$ to 0.5; Petters & Kreidenweis, 2007). This result is in agreement with the measured accumulation mode mass fractions (Figure 10b). In addition, the accumulation mode organics appear to be dissimilar, at least in terms of hygroscopicity, to those in freshly emitted SSA. The range of κ values reported here agree with those previously reported for Pacific Ocean marine atmospheres (Gaston et al., 2018; Roberts et al., 2010).

5. Discussion

A free tropospheric source of particles to the MBL has been recognized for over 20 years (Clarke et al., 1998; Katoshevski et al., 1999; Raes, 1995). Using results from a box model, Raes (1995) hypothesized that the subsidence of free tropospheric particles into the MBL is an important mechanism that can explain observed particle number concentrations. Measurements on the coast of Hawaii revealed that a flux of aerosol from the free troposphere was required to match observed particle concentrations in the clean marine atmosphere (Clarke et al., 2006). More relevant to the North Atlantic, three years of measurements (2015–2017) at the ARM site on Graciosa Island showed that particles entrained from the free troposphere represent the major source of CCN in the MBL, including accumulation mode particles and Aitken mode particles that then undergo condensational growth once in the MBL (Zheng et al., 2018). These previously reported results along with the correlations reported here between LI and CN_5/CN_{13} and LI and the number concentration of nonvolatile particles provide evidence for a free tropospheric source of refractory aerosol over the western North Atlantic that persists over all seasons. This refractory material was observed in the Aitken mode size range after heating to 230 °C but all or a fraction of it could have occurred at larger sizes prior to heating.

The results presented here show that nss $SO_4^=$ dominated the CCN number population in the western North Atlantic MBL in all seasons except November. Nss $SO_4^=$ is also known to have a free tropospheric source. DMS is transported aloft and is oxidized to H_2SO_4 in cloud outflow regions where conditions favor new particle formation (low particle surface area, high relative humidity, and high actinic flux; Clarke, Varner, et al., 1998). Sanchez et al. (2018) estimated that about half of the nss $SO_4^=$-containing particles during both November (NAAMES-1) and May/June (WACS-2 and NAAMES-2) formed in cloud outflow regions and were subsequently entrained into the MBL. The other half resulted from the condensation of sulfate onto existing particles which may also have originated from the free troposphere. As with Aitken mode particles, accumulation mode particles in the MBL are, in large part, a result of atmospheric processing involving entrainment from the free troposphere.

Measurements during WACS-2 and NAAMES showed that the fraction of the total number of particles in the North Atlantic MBL attributable to SSA is low (<10%), except during November when wind speeds were high, phytoplankton concentrations per volume of seawater were low, and atmospheric DMS concentrations were low. However, it should also be noted that the total number concentration during November was relatively low, averaging 77 ± 38 cm^{-3}. These results agree with other recently reported observations of low number concentrations of SSA in the MBL (Blot et al., 2013; Modini et al., 2015; Quinn et al., 2017; Zheng et al., 2018). As a result, with the exception of November, the SSA modal CCN number fractions presented here are low, with average values ranging from 0.13 to 0.31 at 1% S. At 0.3% S, average values ranged between 7 and 19% for March, May/June, and September.

6. Conclusions

The subarctic western North Atlantic is home to the largest, seasonally recurring phytoplankton bloom on Earth. At times, it is also the recipient of air masses arriving from unpolluted regions. It has been hypothesized that during clean marine atmospheric conditions, it should be possible to find a connection between ocean ecosystems and overlying aerosol and cloud properties if one exists. WACS-2 and the four NAAMES experiments were designed to target the seasonality of the plankton bloom with the NAAMES-1 cruise in November targeting the early winter transition event initiating the annual bloom phase, NAAMES-4 in March and April focusing on the phytoplankton accumulation phase, WACS-2 and NAAMES-2 in May and June targeting the bloom climax period, and NAAMES-3 in September studying the declining phase of the bloom. During these experiments, phytoplankton community composition, seawater volume concentrations, and physiological stress as well as chlorophyll concentrations varied widely. Measurements of unheated and heated number size distributions, unheated and heated CCN and CN

concentrations, and aerosol chemical composition were used to assess aerosol and cloud-nucleating properties associated with seasonal changes in the plankton bloom.

The contribution of SSA to the western North Atlantic CCN population was found to be minimal (averaging 14 to 31% at 0.1% S) during March/April, May/June, and September preventing a strong linkage between SSA and overlying cloud properties. The exception was November when atmospheric DMS and nss $SO_4^=$ concentrations were at a minimum and when bloom accumulation had not yet occurred. In contrast, nss $SO_4^=$ was found to be significantly correlated with CCN concentrations indicating that biogenic sulfate provides the sought-after link between ocean ecosystems and aerosol and cloud properties.

Refractory material in the Aitken mode after heating the aerosol to 230 °C was found to be prevalent during all seasons. Based on correlations between the number concentration of nonvolatile particles and the Lifted Index, a measure of atmospheric instability, this refractory material is most likely associated with downward mixing from the free troposphere into the MBL. Hence, atmospheric processing via entrainment of both nonrefractory aerosol and nss $SO_4^=$ from the free troposphere into the MBL appears to have a stronger control on western North Atlantic aerosol than does the response of SSA to surface ocean properties.

Data Availability Statement

All data are available on the NASA data servers accessible through https://naames.larc.nasa.gov and the NOAA PMEL atmospheric chemistry data server accessible through https://saga.pmel.noaa.gov.

Acknowledgments
AcknowledgementsWe thank the officers and crew of the R/V *Ronald H. Brown* and R/V *Atlantis* for their help and commitment during the WACS-2 and NAAMES cruises. This research was funded by the NSF Atmospheric Chemistry Program, the NASA Earth System Science Program, and the NOAA Ocean and Atmospheric Research Office. This is PMEL contribution 5019.

References

Andreae, M. O., Andreae, T. W., Meyerdierks, D., & Thiel, C. (2003). Marine sulfur cycling and the atmospheric aerosol over the springtime North Atllantic. *Chemosphere*, *52*, 1321–1343.

Andreae, M. O., & Rosenfeld, D. (2008). Aerosol-cloud-precipitation interactions. Part 1. The nature and sources of cloud-active aerosols. *Earth-Science Reviews*, *89*, 13–41.

Bates, T. S., Coffman, D. J., Covert, D. S., & Quinn, P. K. (2002). Regional marine boundary layer aerosol size distributions in the Indian, Atlantic and Pacific Oceans: A comparison of INDOEX measurements with ACE-1 and ACE-2, and Aerosols99. *Journal of Geophysical Research*, *107*(D19), 8026. https://doi.org/10.1029/2001JD001174

Bates, T. S., Kapustin, V. N., Quinn, P. K., Covert, D. S., Coffman, D. J., Mari, C., et al. (1998). Processes controlling the distribution of aerosol particles in the lower marine boundary layer during the First Aerosol Characterization Experiment (ACE 1). *Journal of Geophysical Research*, *103*, 16,369–16,383.

Bates, T. S., Quinn, P. K., Frossard, A. A., Russell, L. M., Hakala, J., Petaja, T., et al. (2012). Measurements of ocean derived aerosol off the coast of California. *Journal of Geophysical Research*, *117*, D00V15. https://doi.org/10.1029/2012jd017588

Behrenfeld, M. J. (2010). Abandoning Sverdrup's critical depth hypothesis on phytoplankton blooms. *Ecology*, *91*(4), 977–989.

Behrenfeld, M. J., & Boss, E. (2018). Student's tutorial on bloom hypotheses in the context of phytoplankton annual cycles. *Global Change Biology*, *24*, 55–77.

Behrenfeld, M. J., Doney, S. C., Lima, I., Boss, E. S., & Siegel, D. A. (2013). Annual cycles of ecological disturbance and recovery underlying the siubarctic Atlantic spring plankton bloom. *Global Biogeochemical Cycles*, *27*, 526–540. https://doi.org/10.1002/gbc.20050

Behrenfeld, M. J., Moore, R. H., Hostetler, C. A., Graff, J., Gaube, P., & e. al. (2019). The North Atlantic Aerosol and Marine Ecosystem Study (NAAMES): Science motive and mission overview. *Frontiers*, *6*. https://doi.org/10.3389/fmars.2019.00122

Berner, A., Lurzer, C., Pohl, F., Preining, O., & Wagner, P. (1979). The size distribution of the urban aerosol in Vienna. *Science of the Total Environment*, *13*, 245–261.

Blot, R., Clarke, A. D., Freitag, S., Kapustin, V. N., Howell, S. G., Jensen, J. B., et al. (2013). Ultrafine sea spray aerosol over the southeastern Pacific: Open-ocean contributions to marine boundary layer CCN. *Atmospheric Chemistry and Physics*, *13*, 7263–7278.

Bond, T., Anderson, T. L., & Cambell, D. (1999). Calibration and intercomparison of filter-based measurements of visible light absorption by aerosols. *Aerosol Science and Technology*, *30*, 582–600.

Bond, T., Doherty, S. J., Fahey, D. W., Forster, P. M., Berntsen, T., DeAngelo, B. J., et al. (2013). Bounding the role of black carbon in the climate system: A scientific assessment. *Journal of Geophysical Research: Atmospheres*, *118*, 5380–5552. https://doi.org/10.1002/jgrd.50171

Bopp, L., Resplandy, L., Orr, J. C., Doney, S. C., Dunne, J. P., Gehlen, M., et al. (2013). Multiple stressors of ocean ecosystems in the 21st century: Projections with CMIP5 models. *Biogeosciences*, *10*(2), 3627–3676. https://doi.org/10.5194/bgd-10-3627-2013

Boss, E., & Behrenfeld, M. J. (2010). In situ evaluation of the initiation of the North Atlantic phytoplankton bloom. *Geophysical Research Letters*, *37*, L18603. https://doi.org/10.1029/2010GL044174

Clarke, A., Varner, J. L., Eisele, F., Mauldin, R. L., Tanner, D., & Litchy, M. (1998). Particle production in the remote marine atmosphere: Cloud outflow and subsidence during ACE-1. *Journal of Geophysical Research*, *103*, 16,397–16,409.

Clarke, A. D., Davis, D., Kapustin, V. N., Eisele, F., Chen, G., Paluch, I., et al. (1998). Particle nucleation in the tropical boundary layer and its coupling to marine sulfur sources. *Science*, *282*(5386), 89–92. https://doi.org/10.1126/science.282.5386.89

Clarke, A. D., Owens, S. R., & Zhou, J. C. (2006). An ultrafine sea-salt flux from breaking waves: Implications for cloud condensation nuclei in the remote marine atmosphere. *Journal of Geophysical Research*, *111*, D06202. https://doi.org/10.1029/2005jd006565

Covert, D. S., Kapustin, V. N., Quinn, P. K., & Bates, T. S. (1992). New particle formation in the marine boundary layer. *Journal of Geophysical Research*, *97*, 20,581–20,589.

Galway, J. G. (1956). The lifted index as a predictor of latent instability. *Bulletin of the American Meteological Society*, *37*, 528–529.

Gaston, C. J., Cahill, J. F., Collins, D. B., Suski, K. J., Ge, J. Y., Barkley, A. E., & Prather, K. A. (2018). The cloud nucleating properties and mixing state of marine aerosols sampled along the southern California coast. *Atmosphere*, *9*. https://doi.org/10.3390/atmos9020052

Gondwe, M., Krol, M., Gieskes, W., Klaassen, W., & De Baar, H. (2003). The contribution of ocean-leaving DMS to the global atmospheric burdens of DMS, MSA, SO_2, and nss $SO_4^=$. *Global Biogeochemical Cycles*, *17*(2), 1056. https://doi.org/10.1029/2002GB001937

Hawkins, L. N., & Russell, L. M. (2010). Polysaccharides, proteins, and phytoplankton fragments: Four chemically distinct types of marine primary organic aerosol classified by single particle spectromicroscopy. *Advances in Meteorology*. https://doi.org/10.1155/2010/612132

Heintzenberg, J., Covert, D. S., & van Dingenen, R. (2000). Size distribution and chemical composition of marine aerosols: A compilation and review. *Tellus Series B*, *52*, 1104–1122.

Holland, J. D. (1978). *The chemistry of the atmosphere and oceans*. Hoboken, NJ: John Wiley.

Hoppel, W. A., Frick, G. M., Fitzgerald, J. W., & Larson, R. E. (1994). Marine boundary layer measurements of new particle formation and the effect which nonprecipitating clouds have on the aerosol size distribution. *Journal of Geophysical Research*, *99*, 14,443–14,459.

Katoshevski, D., Nenes, A., & Seinfeld, J. H. (1999). A study of processes that govern the maintenance of aerosol in the marine boundary layer. *Journal of Aerosol Science*, *30*(4), 503–532.

Lance, S., Medina, J., Smith, J. N., & Nenes, A. (2006). Mapping the operation of the DMT continuous flow CCN counter. *Aerosol Science and Technology*, *40*, 242–254.

Lewis, E. R., & Schwartz, S. E. (2004). *Sea salt aerosol production: Mechanisms, methods, measurements, and models—A critical review* (p. 413). Washington, DC: American Geophysical Union.

Modini, R. L., Frossard, A. A., Ahlm, L., Russell, L. M., Corrigan, C. E., Roberts, G., et al. (2015). Primary marine aerosol-cloud interactions off the coast of California. *Journal of Geophysical Research: Atmospheres*, *120*, 4282–4303. https://doi.org/10.1002/2014JD022963

Monahan, E. C., Fairall, C. W., Davidson, K. L., & Boyle, P. J. (1983). Observed inter-relations between 10 m winds, ocean whitecaps, and marine aerosols. *Quarterly Journal of the Royal Meteorological Society*, *109*(460), 379–392.

O'Dowd, C. D., Facchini, M. C., Cavalli, F., Ceburnis, D., Mircea, M., Decesari, S., et al. (2004). Biogenically driven organic contribution to marine aerosol. *Nature*, *431*, 676–680.

Pandis, S. N., Russell, L. M., & Seinfeld, J. H. (1994). The relationship between DMS flux and CCN concentration in remote marine regions. *Journal of Geophysical Research*, *99*, 16,945–16,957.

Pennypacker, S., & Wood, R. (2017). A case study in low aerosol number concentrations over the eastern North Atlantic: Implications for pristine conditions in the remote marine boundary layer. *Journal of Geophysical Research: Atmospheres*, *122*, 12,393–312,415. https://doi.org/10.1002/2017JD027493

Petters, M. D., & Kreidenweis, S. M. (2007). A single parameter representation of hygroscopic growth and cloud condensation nucleus activity. *Atmospheric Chemistry and Physics*, *7*(8), 1961–1971.

Pirjola, L., O'Dowd, C. D., Brooks, I. M., & Kulmala, M. (2000). Can new particle formation occur in the clean marine boundary layer? *Journal of Geophysical Research*, *105*(D21), 26,531–26,546.

Prather, K. A., Bertram, T. H., Grassian, V. H., Deane, G. B., Stokes, M. D., DeMott, P. J., et al. (2013). Bringing the ocean into the laboratory to probe the chemical complexity of sea spray aerosol. *Proceedings of the National Academy of Sciences of the United States of America*, *110*(19), 7550–7555.

Quinn, P. K., & Bates, T. S. (2005). Regional aerosol properties: Comparisons of boundary layer measurements from ACE 1, ACE 2, Aerosols99, INDOEX, ACE Asia, TARFOX, and NEAQS. *Journal of Geophysical Research*, *110*, D14202. https://doi.org/10.1029/2004JD004755

Quinn, P. K., & Bates, T. S. (2011). The case against climate regulation via oceanic phytoplankton sulfur emissions. *Nature Geoscience*, *480*, 51–56.

Quinn, P. K., Coffman, D. J., Bates, T. S., Miller, T. L., Johnson, J. E., Welton, E. J., et al. (2002). Aerosol optical properties during INDOEX 1999: Means, variabilities, and controlling factors. *Journal of Geophysical Research*, *107*(D19), 8020. https://doi.org/10.1029/2000JD000037

Quinn, P. K., Coffman, D. J., Johnson, J. E., Upchurch, L. M., & Bates, T. S. (2017). Small fraction of marine cloud condensation nuclei made up of sea spray aerosol. *Nature Geoscience*, *10*, 674–679.

Quinn, P. K., Coffman, D. J., Kapustin, V. N., Bates, T. S., & Covert, D. S. (1998). Aerosol optical properties in the marine boundary layer during the first Aerosol Characterization Experiment (ACE-1) and the underlying chemical and physical aerosol properties. *Journal of Geophysical Research*, *103*, 16,743–16,751.

Quinn, P. K., Miller, T. L., Bates, T. S., Ogren, J. A., Andrews, E., & Shaw, G. E. (2002). A 3-year record of simultaneously measured aerosol chemical and optical properties at Barrow, Alaska. *Journal of Geophysical Research*, *107*(D11), 4130. https://doi.org/10.1029/2001JD001248

Raes, F. (1995). Entrainment of free-tropospheric aerosol as a regulating mechanism for cloud condensation nuclei in the remote marine boundary layer. *Journal of Geophysical Research*, *100*, 2893–2903.

Rinaldi, M., Decesari, S., Finessi, E., Giulianelli, L., Carbone, C., Fuzzi, S., et al. (2010). Primary and secondary organic marine aerosol and oceanic biological activity: Recent results and new perspectives for future studies. *Advances in Meteorology*, *2010*, 1–10. https://doi.org/10.1155/2010/310682

Roberts, G., Day, D. A., Russell, L. M., Dunlea, E. J., Jimenez, J. L., Tomlinson, J. M., et al. (2010). Characterization of particle cloud droplet activity and composition in the free troposphere and the boundary layer during INTEX-B. *Atmospheric Chemistry and Physics*, *10*, 6627–6644.

Roberts, G., & Nenes, A. (2005). A continuous-flow streamwise thermal gradient CCN chamber for atmospheric measurements. *Aerosol Science and Technology*, *39*, 206–221.

Saltzman, E. S. (2009). Marine aerosols. In *Surface ocean-lower atmosphere processes* (pp. 17–35). Geophysical Monograph Series: American Geophysical Union.

Sanchez, K. J., Chen, C.-L., Russell, L. M., Betha, R., Liu, J., Price, D. J., et al. (2018). Substantial seasonal contribution of observed biogenic sulfate particles to cloud condensation nuclei. *Scientific Reports*, *8*. https://doi.org/10.1038/s41598-018-21590-9

Schauer, J. J., Mader, J. T., Deminter, J. T., Heidemann, G., Bae, M. S., Seinfeld, J. H., et al. (2003). ACE Asia intercomparison of a thermal-optical method for the determination of particle-phase organic and elemental carbon. *Environmental Science & Technology*, *37*, 993–1001.

Seinfeld, J. H., & Pandis, S. N. (2006). *Atmospheric chemistry and physics: From air pollution to climate change* (2nd ed.). New York: John Wiley and Sons.

Siegal, D. A., Buesseler, K. O., Doney, S. C., Sailley, S., Behrenfeld, M. J., & Boyd, P. W. (2014). Global assessment of ocean carbon export using food-web models and satellite observations. *Global Biogeochemical Cycles*, *28*, 181–196. https://doi.org/10.1002/2013GB004743

Stein, A. F., Draxler, R. R., Rolph, G. D., Stunder, B. J. B., Cohen, M. D., & Ngan, F. (2015). NOAA's HYSPLIOT atmospheric transport and dispersion modeling system. *Bulletin of the American Meteological Society*, *96*, 2059–2077.

Stratmann, F., & Wiedensohler, A. (1997). A new data inversion algorithm for DMPS measurements. *Journal of Aerosol Science*, *27*, 339–340.

Takahashi, T., Sutherland, S. C., Wanninkhof, R., & e. al. (2009). Climatological mean and decadal change in surface ocean pCO_2, and net sea–air CO_2 flux over the global oceans. *Deep-Sea Research Part II*, *56*, 554–577.

Turpin, B. J., & Lim, H.-J. (2001). Species contributions to $PM_{2.5}$ mass concentrations: Revisiting common assumptions for estimating organic mass. *Aerosol Science and Technology*, *35*, 602–610.

Wehner, B., Philippin, S., & Wiedensohler, A. (2002). Design and calibration of a thermodenuder with an improved heating unit to measure the size-dependent volatile fraction of aerosol particles. *Journal of Aerosol Science*, *33*, 1087–1093.

Whittlestone, S., & Zahorowski, W. (1998). Baseline radon detectors for shipborad use: Development and deployment in the First Aerosol Characterization Experiment (ACE-1). *Journal of Geophysical Research*, *103*, 16,743–16,751.

Winklmeyer, W., Reischl, G. P., Lindner, A. O., & Berner, A. (1991). New electromobility spectrometer for the measurement of aerosol size distributions in the size range 1 to 1,000 nm. *Journal of Aerosol Science*, *22*, 289–296.

Yoon, Y. J., Ceburnis, D., Cavalli, F., Jourdan, O., Putaud, J.-P., Facchini, M. C., et al. (2007). Seasonal characteristics of the physico-chemical properties of North Atlantic marine atmospheric aerosols. *Journal of Geophysical Research*, *112*, D04206. https://doi.org/10.1029/2005JD007044

Zheng, G., Wang, Y., Aiken, A. C., Gallo, F., Jensen, M. P., Kollias, P., et al. (2018). Marine boundary layer aerosol in the eastern North Atlantic: Seasonal variations and key controlling processes. *Atmospheric Chemistry and Physics*, *18*, 17,615–17,635.